been available for competitive repopulation assay of human HSCs, but a major shortcoming of the NOD/SCID mouse is a lack of reproducible T cell differentiation from $CD34^+$ cells [20–22]. We recently reported that the NOD/SCID/γc^{null} (NOG) mouse, which had been crossed with mice expressing a form of the IL-2Rγ chain lacking the cytoplasmic region, reproducibly develops human T cells, in addition to myeloid, NK, and B-lymphoid cells when transplanted with cord blood $CD34^+$ cells [23–25]. The repopulated T cells bear polyclonal $\alpha\beta$ TCR and respond not only to mitogenic stimuli, such as PHA and IL-2, but also to allogeneic human cells. These results indicate that functional human T lymphocytes can be reconstituted from $CD34^+$ cells in NOG mice. These animals therefore provide a new system in which it is possible to analyze *in vivo* competitive repopulation of the full lymphopoietic system using human HSCs.

Here, we report a novel competitive repopulation system, in which two UCB units were labeled with recombinant lentiviral vectors carrying either an enhanced green fluorescent protein (EGFP)- or an enhanced yellow fluorescent protein (EYFP)-encoding gene to enable easy identification of progeny cells. Using this system, we evaluated competitive repopulation by purified $CD34^+$ cells from two units of UCB with or without cotransplantation of mononuclear cells (MNC) and their purified populations.

RESULTS

Competitive Repopulation of Combined UCB $CD34^+$ Cells Transplanted into the NOG Mouse

We transplanted 11 pairs of UCB $CD34^+$ cells bearing distinct HLA alleles simultaneously into sublethally irradiated NOG mice (Table 1). To distinguish progeny derived from each UCB unit of $CD34^+$ cells, we labeled one unit by transfection with a lentivirus vector containing the EGFP gene and the other unit with a lentivirus vector containing the EYFP gene. After transplantation, we collected peripheral blood (PB) cells retro-orbitally at various intervals and analyzed them by flow cytometry for the presence of human hematopoietic cells expressing the leukocyte common antigen CD45 (Figs. 1A and 1B). Individual progeny from each unit of UCB $CD34^+$ cells were easily identified by the expression of these marker genes.

To evaluate the stability of any chimerism from two UCB donors in mice, we plotted the ratio of $EGFP^+$ to $EYFP^+$ cell number in PB over time after transplantation. Although the transduction efficiencies and numbers of $CD34^+$ cells varied between each experiment, the chimeric ratio of $EGFP^+$ to $EYFP^+$ cells observed at 3 weeks after transplantation was fairly stable up to at least 18 weeks (Fig. 1C). In some experiments, the ratio was stable up to 6 months after transplantation ($n = 3$ analyzed, data not shown).

To evaluate the relative viability of the two UCB donors in mice, we plotted the ratio of $EGFP^+$ to $EYFP^+$

TABLE 1: Characteristics of the CB units

Expt	No. cells ($\times 10^4$)	$CD34^+CD38^-$ (%)	Infection	Transduction efficiency (%)	HLA A	HLA B	HLA DR
1	5.5	10.99	GFP	12.72	2/26	46/60	8/–
	11.4	8.7	YFP	12.11	2/–	51/75	15/–
2	11	5.86	GFP	17.04	1/24	37/52	14/15
	8	4.56	YFP	16.72	2/24	7/35	1/4
3	13.8	10.21	GFP	14.84	24/–	7/61	1/9
	16	4.8	YFP	15.13	2/24	46/–	8/–
4	15.8	4.35	GFP	7.56	24/33	44/52	9/13
	10.5	5.67	YFP	8.13	1/24	37/52	10/15
5	19	6.37	GFP	18.64	2/24	46/62	4/8
	13.9	4.1	YFP	17.87	24/26	7/61	9/13
6	17.5	8.39	GFP	18.76	N.D.	N.D.	N.D.
	24	6.22	YFP	17.81	2/–	59/61	4/–
7	8.75	13.14	GFP	10.35	2/24	35/62	4/11
	4	5.24	YFP	15.84	2/33	51/–	8/9
8	9	14.58	GFP	28.16	24/26	52/62	4/15
	35	5.4	YFP	25.58	2/24	46/61	8/9
9	98	7.57	GFP	25.28	24/33	7/44	1/13
	47	6.84	YFP	26.63	24/–	52/61	9/15
10	18.75	9.24	GFP	25.20	24/26	54/61	4/9
	15.75	4.55	YFP	12.55	11/24	51/62	11/15
11	10.5	17.6	GFP	27.01	24/33	44/52	9/13
	9.5	12.53	YFP	23.84	1/24	37/52	10/15

N.D., not determined. –, blank allele.

doi:10.1016/j.ymthe.2004.07.029

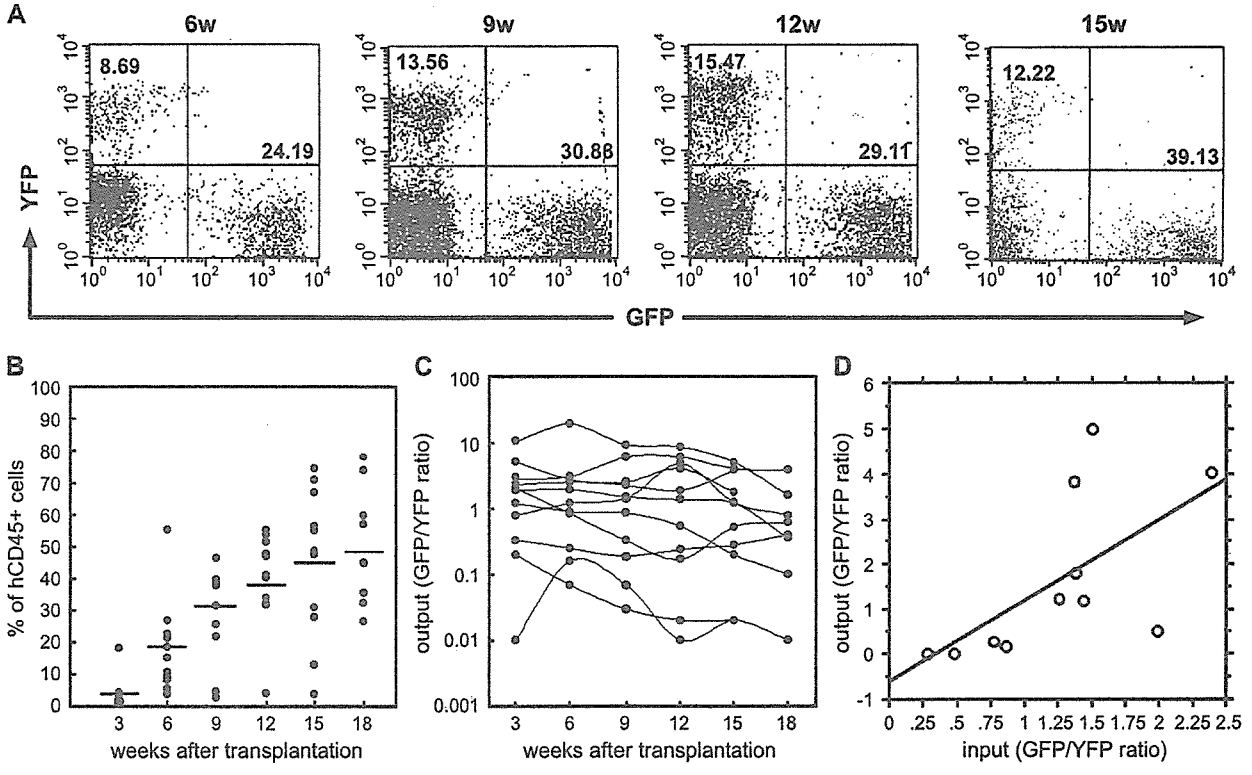

FIG. 1. (A) Representative FACS profiles of competitive repopulation of EGFP- or EYFP-transduced CB CD34$^+$ cells in an individual NOG mouse recipient. PB cells were collected at specific intervals and stained with anti-human CD45 mAb. The stained cells were then analyzed by flow cytometry gated for the expression of CD45. Each donor-derived human hematopoietic cell was distinguished by the expression of the marker EGFP or EYFP. (B) Kinetics of human hematopoietic cells in NOG mice transplanted with two units of CB CD34$^+$ cells. PB cells were collected at various intervals from transplanted NOG mice (n = 11) and stained with anti-human CD45 mAb. Each dot represents one mouse recipient, and bars indicate the average of engraftment. (C) The ratio of each donor's derived CD45$^+$ hematopoietic cells detected in the NOG mouse PB was calculated. (D) A weak linear relationship between the ratio of injected CD34$^+$ cell number (horizontal axis) and the ratio of human hematopoietic cells engrafted in the PB at 15 weeks after transplantation (vertical axis) (r = 0.623, n = 11, P = 0.039).

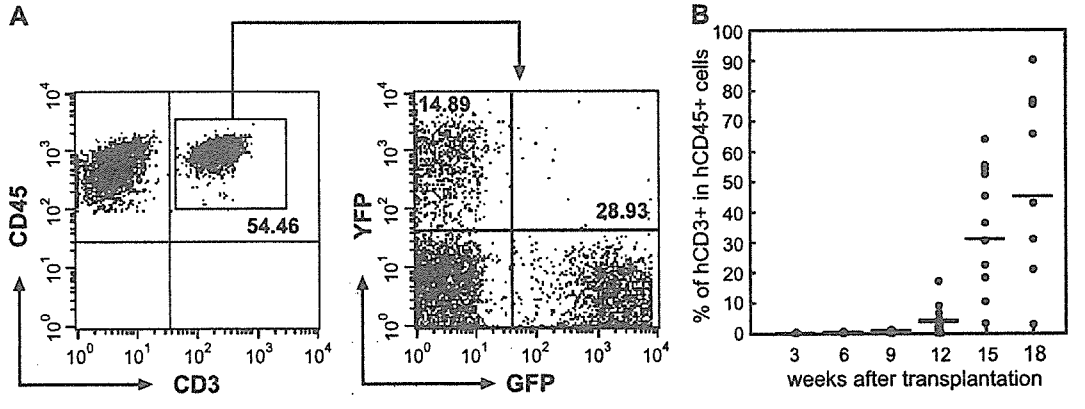

FIG. 2. (A) Representative FACS profiles of CD3$^+$ T lymphocytes in competitive repopulation of EGFP- or EYFP-transduced CB CD34$^+$ cells in an individual NOG mouse recipient. PB cells were collected at 15 weeks after transplantation. Anti-human CD3 mAb and anti-human CD45 mAb were used to detect human T lymphocytes in the PB of engrafted NOG mice. The CD3$^+$CD45$^+$ region was gated and marker gene expression was analyzed. (B) Kinetics of human CD3$^+$ T lymphocytes in NOG mice transplanted with two units of CB CD34$^+$ cells. PB cells were collected at various intervals from transplanted NOG mice (n = 11) and stained with anti-human CD3 mAb and anti-human CD45 mAb. The stained cells were then analyzed by flow cytometry gated for the expression of CD45. Each dot represents one mouse recipient, and bars indicate the average engraftment.

TABLE 2: Lineage analysis of T lymphocytes derived from two UCB units in the thymus of NOG mice

Expt	Phenotype	Lineages (%) DN	DP	$CD4^+$ SP	$CD8^+$ SP
1	$GFP^+/CD45^+$	N.D.	N.D.	N.D.	N.D.
	$YFP^+/CD45^+$	N.D.	N.D.	N.D.	N.D.
3	$GFP^+/CD45^+$	4.11	69.08	14.09	12.72
	$YFP^+/CD45^+$	3.86	66.80	16.22	13.13
4	$GFP^+/CD45^+$	8.00	50.50	26.00	15.50
	$YFP^+/CD45^+$	1.60	65.07	21.60	18.16
6	$GFP^+/CD45^+$	8.90	44.70	27.35	22.72
	$YFP^+/CD45^+$	1.96	67.99	18.22	11.83
7	$GFP^+/CD45^+$	15.17	45.07	18.16	21.6
	$YFP^+/CD45^+$	18.20	43.80	17.22	20.78
9	$GFP^+/CD45^+$	32.64	34.55	12.81	19.99
	$YFP^+/CD45^+$	22.32	20.06	16.47	41.15
10	$GFP^+/CD45^+$	2.03	35.29	28.26	34.42
	$YFP^+/CD45^+$	0.24	44.01	20.45	35.30
11	$GFP^+/CD45^+$	16.55	51.39	18.39	16.55
	$YFP^+/CD45^+$	0.29	38.07	24.08	37.56

N.D., not determined.

cell number in PB against the ratio of engrafted $CD34^+$ cells. There was a linear relationship between the $EGFP^+$ to $EYFP^+$ cell ratio observed at 15 weeks after transplantation and the $EGFP^+$ to $EYFP^+$ $CD34^+$ cell ratio at the time of transplantation ($r = 0.623$, $P = 0.039$, $n = 11$; Fig. 1D). Similarly, the $EGFP^+$ to $EYFP^+$ ratio in engrafted cells in bone marrow (BM) correlated with the $EGFP^+$ to $EYFP^+$ ratio at transplantation ($r = 0.713$, $P = 0.0458$, $n = 8$), although three mice died before the analysis.

These data demonstrate that one unit of UCB $CD34^+$ cells will engraft with the same efficiency in NOG mice regardless of whether a second, different, unit of UCB $CD34^+$ cells is simultaneously transplanted.

Multilineage Differentiation of Two Units of Cord Blood $CD34^+$ cells

Consistent with our previous results [23], we began to detect human $CD3^+$ T lymphocytes at 9 weeks posttransplantation of UCB $CD34^+$ cells and their numbers steadily increased up to 18 weeks (Fig. 2B). Both $EGFP^+$ and $EYFP^+$ $CD3^+$ T lymphocytes were detected in PB of NOG mice between 9 and 18 weeks posttransplantation (Fig. 2A).

Fifteen to 24 weeks after transplantation, we killed the mice and collected the thymus, BM, and spleen to analyze the progeny of the two units of UCB $CD34^+$ cells. In the thymus, most thymocytes in the NOG mice were human $CD3^+$ cells, which had differentiated from both $EGFP^+CD34^+$ cells and $EYFP^+CD34^+$ cells (Table 2 and Fig. 3). Thymocytes from both donors showed normal differentiation patterns, which comprised both double-positive and single-positive subsets of CD4/CD8.

In BM and spleen, we analyzed multilineage differentiation of $EGFP^+CD34^+$ cells and $EYFP^+CD34^+$ cells by gating $EGFP^+CD45^+$ and $EYFP^+CD45^+$ cells. In addition to $CD3^+$ T cells, $CD19^+$ B cells, $CD56^+$ NK cells, $CD14^+$ monocytes, $CD33^+$ myeloid cells, and primitive $CD34^+$ cells arose from both the $EGFP^+CD45^+$ and the $EYFP^+CD45^+$ units (Table 3, Fig. 4, and spleen data not shown).

These data demonstrate that the multilineage engraftment of one unit of UCB $CD34^+$ cells in NOG mice is

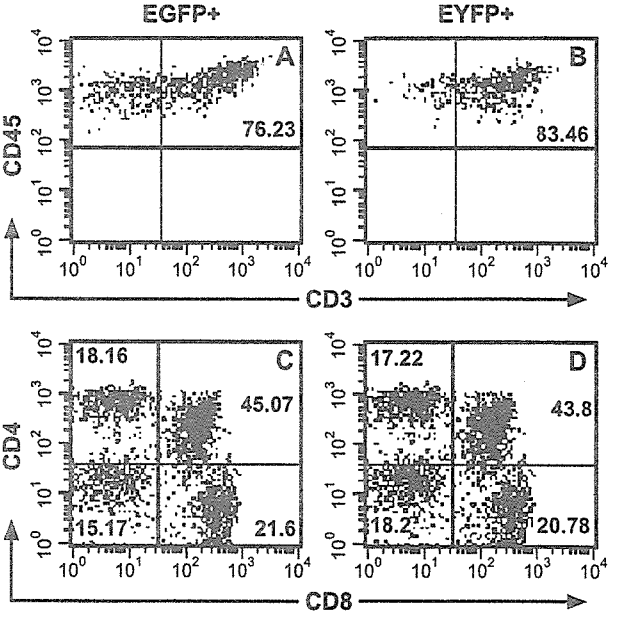

FIG. 3. Representative FACS analysis of human T cell engraftment in the thymus of a NOG mouse recipient transplanted with two combined units of CB $CD34^+$ cells. At 18 weeks after transplantation, thymocytes were collected and stained with anti-human CD45 mAb. Each (A, C) $CD45^+EGFP^+$ and (B, D) $CD45^+EYFP^+$ region was gated, and the expression of (A, B) CD3 and (C, D) CD4/CD8 was analyzed. The relative frequencies of each population are indicated.

doi:10.1016/j.ymthe.2004.07.029

TABLE 3: Lineage analysis of two UCB units of CD34$^+$-derived hematopoietic cells that had differentiated in BM of NOG mice

Expt	Phenotype	Lineages (%) CD14$^+$	CD19$^+$	CD33$^+$	CD34$^+$	CD56$^+$
1	GFP$^+$/CD45$^+$	11.76	38.46	37.27	15.91	4.00
	YFP$^+$/CD45$^+$	12.22	57.47	19.54	12.05	2.33
3	GFP$^+$/CD45$^+$	16.28	34.34	38.26	14.01	4.35
	YFP$^+$/CD45$^+$	18.24	25.07	49.22	16.47	8.13
4	GFP$^+$/CD45$^+$	9.21	21.37	10.16	10.29	0.88
	YFP$^+$/CD45$^+$	10.76	29.86	12.63	10.72	1.61
6	GFP$^+$/CD45$^+$	24.44	11.18	37.77	3.36	4.75
	YFP$^+$/CD45$^+$	10.97	46.70	13.52	5.86	8.04
7	GFP$^+$/CD45$^+$	17.17	62.97	28.72	18.91	1.32
	YFP$^+$/CD45$^+$	12.85	48.52	20.42	9.49	2.55
9	GFP$^+$/CD45$^+$	5.25	18.37	11.13	6.44	6.17
	YFP$^+$/CD45$^+$	17.19	37.23	31.25	6.60	7.23
10	GFP$^+$/CD45$^+$	5.33	24.63	10.65	3.22	2.98
	YFP$^+$/CD45$^+$	3.06	18.24	3.70	3.93	2.67
11	GFP$^+$/CD45$^+$	10.78	52.72	13.51	3.90	2.25
	YFP$^+$/CD45$^+$	26.24	29.46	7.44	9.76	1.06

stable and unaffected by lymphopoietic repopulation by another UCB unit.

Effects of Cotransplantation of CD34$^-$ Mononuclear Cells on Competitive Repopulation in The NOG Mouse

Unfractionated UCB cells containing mature immune-competent cells are commonly used in clinical UCBT. These cells can induce graft-versus-host, graft-versus-tumor, and graft-versus-graft reactions. The effects of the latter reaction on engraftment in particular are poorly understood in m-UCBT. To assess these effects, we performed three sets of competitive repopulation assay by cotransplantation of pairs of CD34$^-$ MNC with EGFP$^+$CD34$^+$ cells and EYFP$^+$CD34$^+$ cells (Table 4).

Four to 6 weeks posttransplantation, we sacrificed the mice and analyzed the ratio of engrafted EGFP$^+$CD45$^+$ and EYFP$^+$CD45$^+$ cells in BM MNC by flow cytometry. When only purified CD34$^+$ cells were transplanted, both UCB units engrafted as expected. However, when CD34$^-$ MNCs were cotransplanted with CD34$^+$ cells, only CD45$^+$ cells from one or the other UCB engrafted in all mice analyzed (Fig. 5). These results indicate that CD34$^-$ MNC from one UCB somehow inhibited engraftment of cells from the other UCB.

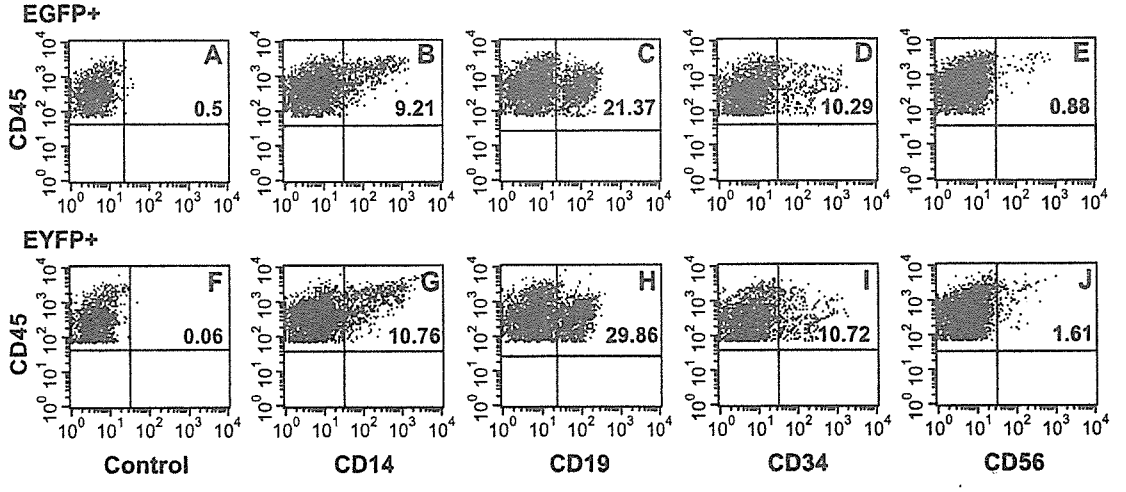

FIG. 4. Representative FACS profile of human multilineage engraftment in a NOG mouse recipient transplanted with two combined units of CB CD34$^+$ cells. At 18 weeks after transplantation, BM cells were collected and analyzed for multilineage differentiation of engrafted human hematopoietic cells. To distinguish hematopoietic cells derived from each donor, each (A–E) CD45$^+$EGFP$^+$ and (F–J) CD45$^+$EYFP$^+$ region was gated, and the percentage of human CD45$^+$ cells expressing the respective surface markers was measured. Human lineage-specific mAbs were used to detect (B, G) myeloid CD45$^+$CD14$^+$, (C, H) lymphoid CD45$^+$CD19$^+$, (E, J) CD45$^+$CD56$^+$, and (D, I) immature CD34$^+$ progenitor cells in the marrow of engrafted NOG mice. The relative frequencies of each population are indicated.

TABLE 4: Characteristics of purified $CD34^+$ cells and MNCs in each CB unit

Expt	Infection	$CD34^+$/mouse ($\times 10^4$)	MNC/mouse ($\times 10^6$)	HLA A	HLA B	HLA DR	HLA DRw
1	GFP	6.0	7.4	2/–	59/61	4/–	53/–
	YFP	6.0	8.8	2/24	51/67	9/12	52/53
2	GFP	12	1.0	2/24	7/51	1/9	53/–
	YFP	7.3	1.0	24/33	44/75	4/13	52/53
3	GFP	16	1.0	24/–	60/–	11/13	52/–
	YFP	11	1.0	2/24	7/61	1/9	53/–

–, blank allele.

To clarify the cell population responsible for this inhibitory effect, we cotransplanted purified $CD4^+$ or $CD8^+$ T lymphocytes or CD4/CD8 double-negative (DN) cells with $EGFP^+CD34^+$ cells and $EYFP^+CD34^+$ cells into NOG mice (Table 5). Although $CD34^-$ MNCs eliminated either $EGFP^+CD45^+$ or $EYFP^+CD45^+$ cells as expected, there was no inhibition of engraftment of $EGFP^+CD45^+$ or $EYFP^+CD45^+$ cells by purified $CD4^+$ or $CD8^+$ T lymphocytes or CD4/CD8 double-negative cells in any mice (Fig. 6). These results indicate that a combination of two or more populations of $CD4^+$, $CD8^+$, and/or DN cells is required for this inhibitory effect.

To determine the effects of a combination of two populations on engraftment, we cotransplanted $EGFP^+CD34^+$ cells and $EYFP^+CD34^+$ cells with combined populations of $CD4^+$ and $CD8^+$ cells, $CD4^+$ and DN cells, and $CD8^+$ and DN cells into NOG mice (Table 6). Both $CD4^+$ and $CD8^+$ cells from one donor cooperated to inhibit engraftment of cells from the other donor, as we observed with whole $CD34^-$ MNC cotransplantation (Fig. 7A). There was no inhibition of engraftment of $EGFP^+CD45^+$ or $EYFP^+CD45^+$ cells by the combination of $CD4^+$ and DN cells or $CD8^+$ and DN cells (Fig. 7B).

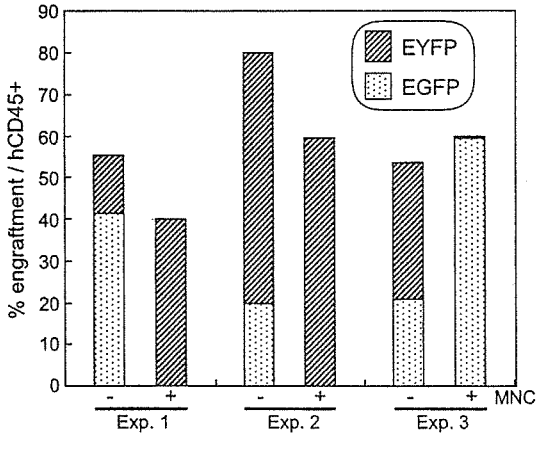

FIG. 5. The effects of $CD34^-$ MNCs on competitive repopulation by $CD34^+$ cells in the NOG mouse. EGFP- or EYFP-transduced $CD34^+$ cells with or without a respective fraction of $CD34^-$ MNCs were injected into the same NOG mouse (Table 4). At 4 to 6 weeks after transplantation, the ratio of engrafted donor-derived hematopoietic cells from each unit was measured using the expression of CD45 and the marker genes in flow cytometry. To exclude residual human T cells derived from $CD34^-$ MNCs, $CD3^+$ cells were gated out at FACS analysis. Data shown are the ratios of $CD45^+EGFP^+$ and $CD45^+EYFP^+$ cells in the BM MNCs of the same NOG recipient (three independent experiments).

Discussion

The possibility of competitive reconstitution of the hematopoietic system by HSCs from multiple UCB units in clinical m-UCBT raises several important questions. Do immune-competent cells developed from two unrelated HSCs affect hematopoietic engraftment or reconstitution in a host? Do mature immune-competent cells derived from two UCB units affect hematopoietic engraftment or reconstitution in a host? To address these questions, we used a novel *in vivo* competitive repopulation system using NOG mice that allows complete reconstitution of human lymphocytes, including T cells, from $CD34^+$ UCB that respond to both mitogenic stimuli, such as PHA and IL-2, and allogeneic human cells [23,25].

We demonstrated here that hematopoietic cells derived from two UCB units engrafted stably, even after $CD3^+$ T cells were detected in recipient PB at 12 weeks after transplantation, and that the ratio of chimerism between cells derived from the two UCB units was correlated with the ratio of cells at transplantation (Fig. 1). Recently, Kim *et al.* [26] demonstrated that two lineage-depleted UCB units could coengraft in NOD/SCID mice. However, this assay could not assess the effects of an immune system derived from HSCs on engraftment by the other, since T cells did not differentiate from $CD34^+$ cells in NOD/SCID mice. Therefore, this is the first demonstration that human immune-competent cells from two immunologically distinct $CD34^+$ donor stem cells can develop normally in the same host environment without inhibiting each other. In recipient NOG mouse thymus, both $EGFP^+CD3^+$ and $EYFP^+CD3^+$ cells showed a normal pattern of T cell differentiation, which comprised both double-positive and single-positive CD4/CD8 subsets (Fig. 4 and Table 2). This suggests that there may have been negative selection in the clonal deletion of cells reactive to each other. Therefore, the content of HSCs may be a good predictor of the resultant chimerism in a mouse, as shown in Fig. 1D.

doi:10.1016/j.ymthe.2004.07.029

TABLE 5: Characteristics of purified CD34$^+$ cells and effector cells in each CB unit

Expt	Infection	CD34$^+$ cells[a]	MNC fraction[b]	HLA A	HLA B	HLA DR	HLA DRw
1	GFP	+	+	2/31	51/54	4/15	51/53
	YFP	+	–	2/33	39/44	9/13	52/53
2	GFP	+	–	11/24	54/67	4/8	53/–[c]
	YFP	+	+	2/24	35/62	9/12	52/53
3	GFP	+	+	2/24	35/61	4/8	53/–
	YFP	+	–	2/26	35/61	9/15	51/53

[a] EGFP- or EYFP-transduced CD34$^+$ cells were transplanted into the same NOG mouse (range of transplanted cell dose 6.8–9 × 10^4 cells).
[b] Unfractionated MNCs (range 7–10 × 10^5 cells), CD4$^+$ cells (range 3.3–5 × 10^5 cells), CD8$^+$ cells (range 1.4–2 × 10^5 cells), and CD4/CD8 double-negative fraction (range 2–3 × 10^5 cells) were prepared from one CB CD34$^-$ fraction (+) and injected into NOG mice together with CD34$^+$ cells derived from the same donor and CD34$^+$ cells derived from the second unit of CB (–).
[c] –, blank allele.

In clinical m-UCBT, the transplanted whole MNC can induce a rapid graft-versus-graft reaction. One study reported successful engraftment of only 1 of 12 randomly selected units of UCB [7]. Another study demonstrated that only one of the two UCB donors was responsible for hematopoiesis in 16 of 18 patients with sustained engraftment [27]. However, another study found that both of the transplanted UCBs contributed to stable hematopoiesis, and this success was attributed to the grafts being closely matched, with only a single mismatch between them at one HLA-DRB1 allele [8]. In the present study, we observed engraftment of either of mismatched pairs of UCB units (Tables 4 and 5), confirming the utility of this animal model to analyze engraftment and hematopoiesis in m-UCBT. We also observed that graft-versus-graft reaction was associated with the CD34$^-$ mononuclear cells in a cord blood unit. In future experiments it would be of interest to analyze the chimerism when an HLA-matched UCB pair is cotransplanted.

One possible drawback to our model is the potential antigenicity of the marker genes EGFP and EYFP used to identify the transplanted cell populations. These two proteins have very similar antigenic properties, since EYFP is simply a mutant form of EGFP [28]; therefore any specific immune reaction would be expected to have an equivalent effect on both cell populations. However, in every case shown in Figs. 5, 6, and 7 either EGFP$^+$ or EYFP$^+$ cells were eliminated, suggesting that this was due to an allospecific reaction.

To identify further the cell population responsible for graft-versus-graft reaction, we cotransplanted purified populations of CD4$^+$, CD8$^+$, or DN cells from two UCBs together with CD34$^+$ cells, but none of these cell populations alone was sufficient to generate a reaction against the other UCB unit (Fig. 6). This suggests that perhaps two populations of effector cells are needed to induce a graft-versus-graft reaction. Consistent with this, we could reproduce this inhibitory effect on engraftment by CD34$^-$ mononuclear cells only when both CD4$^+$ and CD8$^+$ cells were transplanted simultaneously (Fig. 7). These results support the hypothesis that graft-reactive CD8$^+$ CTL served as the terminal effector cell in the rejection, while CD4$^+$ cells provided the signals required for CTL development and expansion [29]. As the strongest alloreaction is provoked by major histocompatibility complex (MHC) antigens, T cells recognize the alloantigens either "directly" as foreign antigens or "indirectly" as presented by self-MHC molecules [30,31]. Our results may suggest that CD4$^+$ and CD8$^+$ T cells from one graft recognized the MHC antigens from the other directly as nonself and then eliminated hematopoietic cells of the other graft, since DN cells were not required as antigen-presenting cells to elicit the reaction. However, Kim and colleagues demonstrated that the mixed transplantation

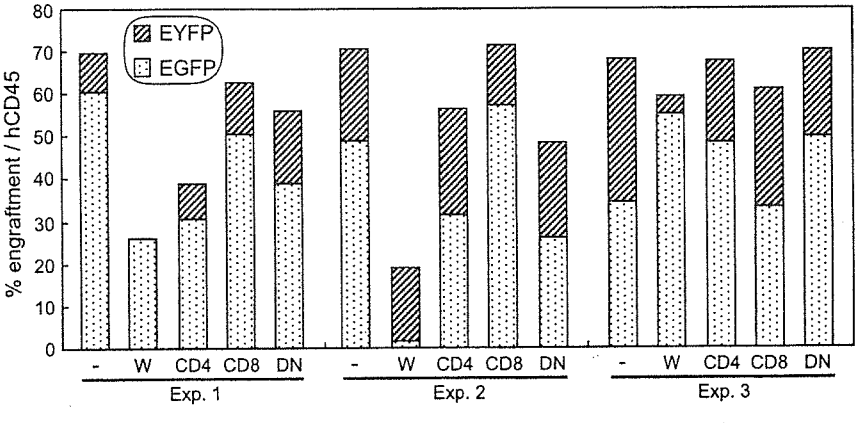

FIG. 6. The effects of fractionated effector cells contained in CD34$^-$ MNCs on competitive repopulation by CD34$^+$ cells in the NOG mouse. CD4$^+$ or CD8$^+$ T lymphocytes and the CD4/CD8 double-negative fraction were sorted from one CB CD34$^-$ fraction and injected into NOG mice together with CD34$^+$ cells derived from the same CB and CD34$^+$ cells derived from the second unit of CB (Table 5). At 3 weeks after transplantation, the ratio of engraftment was analyzed by the same method as for Fig. 5. Data shown are the ratios of CD45$^+$EGFP$^+$ and CD45$^+$EYFP$^+$ cells in the BM MNCs of the same NOG recipient (three independent experiments). (–) Transplants without CD34$^-$ MNCs; (W) transplants with whole CD34$^-$ MNC.

TABLE 6: Characteristics of purified $CD34^+$ cells and effector cells in each CB unit

Expt	Infection	$CD34^+$ cells[a]	MNC fraction[b]	HLA A	HLA B	HLA DR	HLA DRw
1	GFP	+	–	2/31	35/–[c]	12/15	51/52
	YFP	+	+	24/26	51/62	4/15	51/53
2	GFP	+	+	2/31	46/61	8/15	51/–
	YFP	+	–	2/24	35/55	4/9	53/–
3	GFP	+	+	24/33	44/75	8/9	53/–
	YFP	+	–	11/–	44/59	4/13	52/53

[a] EGFP- or EYFP-transduced $CD34^+$ cells (5×10^4 cells) were transplanted into the same NOG mouse.
[b] Unfractionated MNCs (10×10^5 cells), $CD4^+$ cells (5×10^5 cells), $CD8^+$ cells (2×10^5 cells), and CD4/CD8 double-negative fraction (range $2–3 \times 10^5$ cells) were prepared from one CB $CD34^-$ fraction (+). Each fraction were combined as $CD4^+$ and $CD8^+$ cells, $CD4^+$ and DN cells, and $CD8^+$ and DN cells and transplanted into NOG mice together with $CD34^+$ cells derived from the same donor and $CD34^+$ cells derived from the second unit of CB (–).
[c] –, blank allele.

of two allogeneic UCB grafts led to single-donor predominance independent of the degree of HLA compatibility between the two grafts [26]. Further investigation is necessary to determine how $CD4^+$ and $CD8^+$ cells contribute to predominant engraftment of HSCs, through either direct recognition of the MHC antigens or other nonspecific effects.

We have established a novel *in vivo* competitive repopulation assay using a new NOG mouse system that may facilitate study of the behavior of different units of stem cells after transplantation. Furthermore, we clearly demonstrated that the lentiviral gene marking strategy can easily distinguish the two distinct donor cells by flow cytometric analysis, independent of

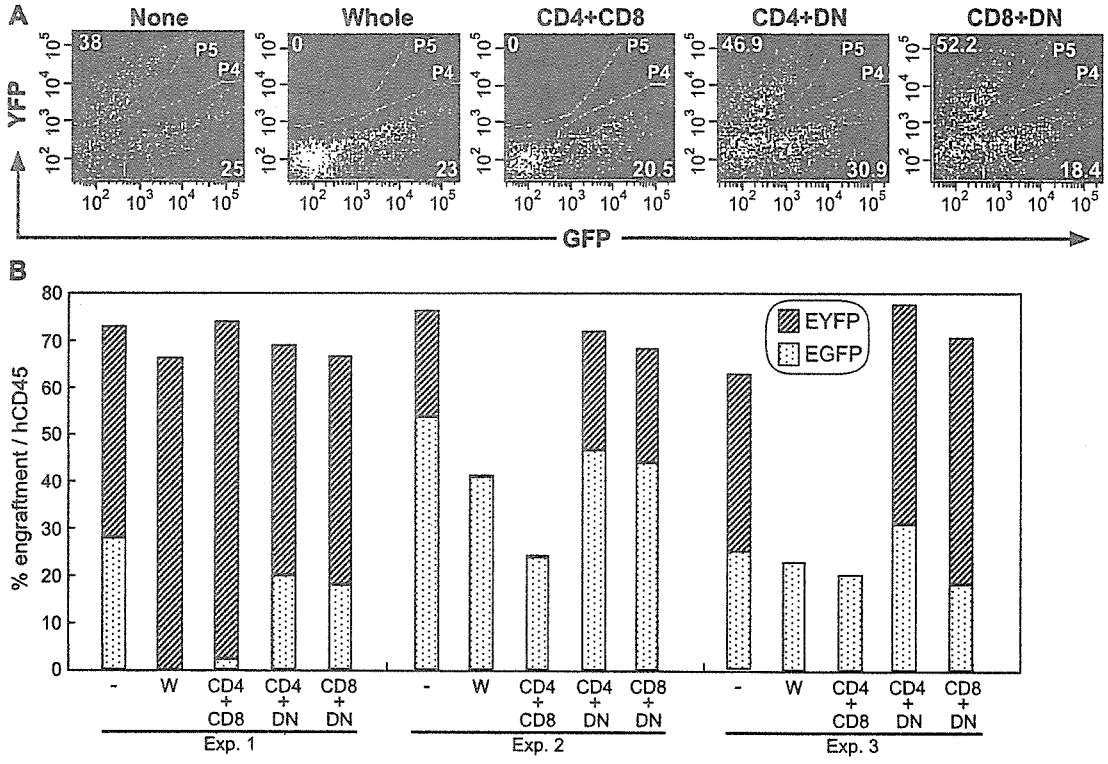

FIG. 7. The effects of combined cell populations contained in $CD34^-$ MNCs on competitive repopulation by $CD34^+$ cells in the NOG mouse. $CD4^+$ and $CD8^+$ T lymphocytes and the CD4/CD8 double-negative fraction were sorted from one CB $CD34^-$ fraction. Each sorted fraction was combined to give $CD4^+$ and $CD8^+$ cells, $CD4^+$ and DN cells, or $CD8^+$ and DN cells and injected into NOG mice together with $CD34^+$ cells derived from the same CB and $CD34^+$ cells derived from the second unit of CB (Table 6). At 3 weeks after transplantation, the ratio of engraftment was analyzed by the same method as for Fig. 5. (A) Representative FACS profiles of competitive repopulation of EGFP- or EYFP-transduced CB $CD34^+$ cells in an individual NOG mouse recipient. (B) Summary of three independent experiments. Data shown are the ratios of $CD45^+EGFP^+$ and $CD45^+EYFP^+$ cells in the BM MNCs of the same NOG recipient. (–) Transplants without $CD34^-$ MNCs; (W) transplants with whole $CD34^-$ MNC.

doi:10.1016/j.ymthe.2004.07.029

cell surface antigens, expression of intracellular isoenzymes, or hemoglobin subtypes. This strategy is also useful for the examination of the stem cell competitive repopulation activity of variety cell sources such as BM cells and cord blood cells, *ex vivo* expanded cells, and nonexpanded cells. Gene transduction by lentiviral infection did not have any apparent untoward effects on the behavior of HSCs, such as multilineage differentiation and long-term repopulation.

We hope that the *in vivo* assay system described here will be useful, not only for examining the competitive hematopoietic repopulation from multiple UCB units, but also for predicting the effects of MNCs cotransplanted in clinical m-UCBT. To evaluate the relevance of this system as a surrogate human HSC assay, it will be important to correlate the results of engraftment in this model with engraftment in clinical m-UCBT.

Materials and Methods

Cells. CB samples were obtained from full-term deliveries following institutional guidelines approved by the Tokai University Committee on Clinical Investigation. MNCs were isolated by Ficoll–Hypaque (Lymphoprep, 1.077 ± 0.001 g/ml; Nycomed, Oslo, Norway) density gradient centrifugation. Cells were washed and suspended in phosphate-buffered saline (PBS) containing 0.1% of human serum globulin (Sigma, St. Louis, MO, USA). $CD34^+$ cell fractions were prepared from Ficoll-separated MNCs using the CD34 Progenitor Cell Isolation Kit (Miltenyi Biotec, Sunnyvale, CA, USA) according to the manufacturer's directions. The enriched $CD34^+$ cell fraction was stained either with fluorescein isothiocyanate (FITC)-conjugated anti-CD34 mAb (581; Coulter/Immunotech, Marseille, France) or with allophycocyanin (APC)-conjugated anti-CD3 mAb (UCHT1; Coulter/Immunotech). $CD34^+CD3^-$ cells were sorted using a FACSVantage flow cytometer (BD Biosciences, San Jose, CA, USA) equipped with HeNe and argon lasers. This resulted in a highly purified $CD34^+$ cell fraction (more than 99%) in which no $CD3^+$ cells were detected on FACS analysis. Sorted $CD34^+CD3^-$ cells were cryopreserved in liquid nitrogen until use. Column passthrough $CD34^-$ MNC fractions were also cryopreserved. On the day of transplantation, cryopreserved $CD34^-$ MNC fractions were thawed and stained with PE-conjugated anti-CD4 (SK3) and FITC-conjugated anti-CD8 (SK1) mAbs (all BD Biosciences). Stained cells were sorted using the FACSVantageSE Diva option (BD Biosciences) gated on each $CD4^+CD8^-$, $CD4^-CD8^+$, and $CD4^-CD8^-$ region. Purified populations were >98% pure. Dead cells stained with PI were excluded from the analysis. The HLA of each CB unit was determined by molecular typing using a Micro SSP HLA Classes I and II ABDR DNA Typing Tray (One Lambda, Canoga Park, CA, USA).

Lentivirus infection. Transduction of the EGFP or its yellow variant EYFP gene into $CD34^+$ cells by recombinant lentivirus infection was performed as described previously [32,33]. Briefly, cryopreserved CB $CD34^+$ cells were thawed and prestimulated by incubation in StemPro-34 medium (Invitrogen, Carlsbad, CA, USA) containing cytokines at 37°C in 5% CO_2 for 24 h. Recombinant human thrombopoietin (50 ng/ml; kindly donated by Kirin Brewery, Tokyo, Japan), stem cell factor (50 ng/ml; donated by Kirin Brewery), and Flk-2/Flt-3 ligand (50 ng/ml; R&D Systems, Minneapolis, MN, USA) were used. Prestimulated $CD34^+$ cells were cultured for 12 h under the same conditions in the presence of highly concentrated lentivirus supernatant at an m.o.i. of 50. Lentivirus-infected $CD34^+$ cells were transplanted into irradiated NOG mice. The efficiency of infection was determined by FACS analysis on the day of transplantation.

Mice. NOG mice were obtained from the Central Institute for Experimental Animals (Kawasaki, Japan) and were maintained in the animal facility of the Tokai University School of Medicine in microisolator cages with autoclaved food and water. Seven- to nine-week-old NOG mice were irradiated with 250 cGy of X-rays and thereafter received acidified water containing 1.1 g/L neomycin sulfate and 131 mg/L polymyxin B sulfate (Sigma). The following day, two units of CB $CD34^+CD3^-$ cells were simultaneously injected intravenously into NOG mice. In some experiments, $CD34^-$ MNCs were cotransplanted with $CD34^+$ cells. All experiments were approved by the animal care committee of Tokai University.

Flow cytometric analysis. For kinetic analysis, mice were anesthetized with ethyl ether and PB samples were aspirated from the retro-orbital sinus. Samples were prepared as single-cell suspensions in PBS containing 0.1% human serum globulin and heparin. Human hematopoietic cells were distinguished from mouse cells by expression of human CD45. At the time of sacrifice, BM, spleen, and PB were collected for analysis of the presence of human cells by flow cytometry. BM cells were suspended in PBS using a 27-gauge needle. Spleen was teased apart, and PB was aspirated from the retro-orbital sinus. Samples were prepared as single-cell suspensions in PBS containing 0.1% human serum globulin and passed through a nylon filter to remove debris. Cells were stained with mAbs to human leukocyte differentiation antigens. APC-conjugated anti-human CD3, CD4, CD14, CD19, CD33, CD34, and CD56 mAbs (all Coulter/Immunotech) and ECD-conjugated anti-human CD8 and CD45 mAbs (all Coulter/Immunotech) were used. Four-color flow cytometric analysis was conducted using FACSVantage (BD Biosciences). Quadrants were set to include at least 97% of the isotype-negative cells. The proportion of each lineage was calculated from 20,000 events acquired using CELLQuest or FACSDiva software (BD Biosciences).

Statistical analysis. Results are expressed as individual data. Input (transplanted EGFP/EYFP ratio) and output (engrafted EGFP/EYFP ratio) were calculated by the following calculation: input (EGFP/EYFP ratio) = (EGFP transplanted cell number × infection efficiency)/(EYFP transplanted cell number × infection efficiency). Output (EGFP/EYFP ratio) = (percentage of $CD45^+EGFP^+$ cells in the recipient)/(percentage of $CD45^+EYFP^+$ cells in the recipient). The correlation of input values and output values was analyzed using StatView-J4.02 software (Abacus Concepts, Berkeley, CA, USA). P values <0.05 were considered to be significant.

Acknowledgments

We thank Hiroyuki Miyoshi, BioResource Center, RIKEN Tsukuba Institute, for the gift of lentivirus vectors; Tatsuya Sugimoto, Center for Cell Transplantation and Regenerative Medicine of Tokai University School of Medicine, for HLA typing; and members of the animal facility of Tokai University, especially Mayumi Nakagawa and Shinya Fujikawa for their meticulous care of experimental animals; and members of the Tokai Cord Blood Bank for their assistance. We also thank members of the Research Center for Regenerative Medicine of Tokai University School of Medicine for their useful discussions and assistance. This work was supported by a Research Grant-in-Aid from the Science Frontier Program from the Ministry of Education, Science, Sports, and Culture of Japan and a Sciences Research Grant from the Ministry of Health and Labor of Japan.

RECEIVED FOR PUBLICATION MARCH 26, 2004; ACCEPTED JULY 22, 2004.

References

1. Broxmeyer, H. E., *et al.* (1992). Growth characteristics and expansion of human umbilical cord blood and estimation of its potential for transplantation in adults. *Proc. Natl. Acad. Sci. USA* **89:** 4109–4113.
2. Gluckman, E., *et al.* (1989). Hematopoietic reconstitution in a patient with Fanconi's anemia by means of umbilical-cord blood from an HLA-identical sibling. *N. Engl. J. Med.* **321:** 1174–1178.
3. Gluckman, E., *et al.* (1997). Outcome of cord-blood transplantation from related and unrelated donors. *N. Engl. J. Med.* **337:** 373–381.

4. Rubinstein, P., *et al.* (1998). Outcomes among 562 recipients of placental-blood transplants from unrelated donors. *N. Engl. J. Med.* **339:** 1565–1577.
5. Gluckman, E. (2001). Hematopoietic stem-cell transplants using umbilical-cord blood. *N. Engl. J. Med.* **344:** 1860–1861.
6. Grewal, S. S., Barker, J. N., Davies, S. M., and Wagner, J. E. (2003). Unrelated donor hematopoietic cell transplantation: marrow or umbilical cord blood? *Blood* **101:** 4233–4244.
7. Weinreb, S., *et al.* (1998). Transplantation of unrelated cord blood cells. *Bone Marrow Transplant* **22:** 193–196.
8. Barker, J. N., Weisdorf, D. J., and Wagner, J. E. (2001). Creation of a double chimera after the transplantation of umbilical-cord blood from two partially matched unrelated donors. *N. Engl. J. Med.* **344:** 1870–1871.
9. Barker, J. N., Weisdorf, D. J., DeFor, T. E., Blazar, B. R., Miller, J. S., and Wagner, J. E. (2003). Rapid and complete donor chimerism in adult recipients of unrelated donor umbilical cord blood transplantation after reduced intensity conditioning. *Blood* **102:** 1915–1919.
10. Szilvassy, S. J., Humphries, R. K., Lansdorp, P. M., Eaves, A. C., and Eaves, C. J. (1990). Quantitative assay for totipotent reconstituting hematopoietic stem cells by a competitive repopulation strategy. *Proc. Natl. Acad. Sci. USA* **87:** 8736–8740.
11. Rebel, V. I., Miller, C. L., Eaves, C. J., and Lansdorp, P. M. (1996). The repopulation potential of fetal liver hematopoietic stem cells in mice exceeds that of their liver adult bone marrow counterparts. *Blood* **87:** 3500–3507.
12. Szilvassy, S. J., Weller, K. P., Chen, B., Juttner, C. A., Tsukamoto, A., and Hoffman, R. (1996). Partially differentiated ex vivo expanded cells accelerate hematologic recovery in myeloablated mice transplanted with highly enriched long-term repopulating stem cells. *Blood* **88:** 3642–3653.
13. Goerner, M., Bruno, B., McSweeney, P. A., Buron, G., Storb, R., and Kiem, H. P. (1999). The use of granulocyte colony-stimulating factor during retroviral transduction on fibronectin fragment CH-296 enhances gene transfer into hematopoietic repopulating cells in dogs. *Blood* **94:** 2287–2292.
14. Kiem, H. P., *et al.* (1997). Gene transfer into marrow repopulating cells: comparison between amphotropic and gibbon ape leukemia virus pseudotyped retroviral vectors in a competitive repopulation assay in baboons. *Blood* **90:** 4638–4645.
15. Hematti, P., Sellers, S. E., Agricola, B. A., Metzger, M. E., Donahue, R. E., and Dunbar, C. E. (2003). Retroviral transduction efficiency of G-CSF+SCF-mobilized peripheral blood CD34$^+$ cells is superior to G-CSF or G-CSF+Flt3-L-mobilized cells in nonhuman primates. *Blood* **101:** 2199–2205.
16. McCune, J. M., Namikawa, R., Kaneshima, H., Shultz, L. D., Lieberman, M., and Weissman, I. L. (1988). The SCID-hu mouse: murine model for the analysis of human hematolymphoid differentiation and function. *Science* **241:** 1632–1639.
17. Larochelle, A., *et al.* (1996). Identification of primitive human hematopoietic cells capable of repopulating NOD/SCID mouse bone marrow: implications for gene therapy. *Nat. Med.* **2:** 1329–1337.
18. Bhatia, M., Wang, J., Kapp, U., Bonnet, D., and Dick, J. E. (1997). Purification of primitive human hematopoietic cells capable of repopulating immune-deficient mice. *Proc. Natl. Acad. Sci. USA* **94:** 5320–5325.
19. Guenechea, G., Gan, O. I., Dorrell, C., and Dick, J. E. (2001). Distinct classes of human stem cells that differ in proliferative and self-renewal potential. *Nat. Immunol.* **2:** 75–82.
20. Shultz, L. D., *et al.* (1995). Multiple defects in innate and adaptive immunologic function in NOD/LtSz-scid mice. *J. Immunol.* **154:** 180–191.
21. Greiner, D. L., Hesselton, R. A., and Shultz, L. D. (1998). SCID mouse models of human stem cell engraftment. *Stem Cells* **16:** 166–177.
22. Kollet, O., *et al.* (2000). Beta2 microglobulin-deficient (B2m(null)) NOD/SCID mice are excellent recipients for studying human stem cell function. *Blood* **95:** 3102–3105.
23. Yahata, T., *et al.* (2002). Functional human T lymphocyte development from cord blood CD34$^+$ cells in nonobese diabetic/Shi-scid, IL-2 receptor gamma null mice. *J. Immunol.* **169:** 204–209.
24. Ito, M., *et al.* (2002). NOD/SCID/gamma(c) (null) mouse: an excellent recipient mouse model for engraftment of human cells. *Blood* **100:** 3175–3182.
25. Hiramatsu, H., *et al.* (2003). Complete reconstitution of human lymphocytes from cord blood CD34$^+$ cells using the NOD/SCID/gamma c null mice model. *Blood* **102:** 873–880.
26. Kim, D. W., Chung, Y. J., Kim, T. G., Kim, Y. L., and Oh, I. H. (2004). Cotransplantation of third-party mesenchymal stromal cells can alleviate single-donor predominance and increase engraftment from double cord transplantation. *Blood* **103:** 1941–1948.
27. Barker, J. N., Weisdorf, D. J., DeFor, T. E., McGlave, P. B., and Wagner, J. E. (2002). Multiple unit unrelated donor umbilical cord blood transplantation in high risk adults with hematologic malignancies: impact on engraftment and chimerism. *Blood* **100:** 41a.
28. Ormo, M., Cubitt, A. B., Kallio, K., Gross, L. A., Tsien, R. Y., and Remington, S. J. (1996). Crystal structure of the Aequorea victoria green fluorescent protein. *Science* **273:** 1392–1395.
29. Gill, R. G. (1993). T-cell–T-cell collaboration in allograft responses. *Curr. Opin. Immunol.* **5:** 782–787.
30. Hernandez-Fuentes, M. P., Baker, R. J., and Lechler, R. I. (1999). The alloresponse. *Rev. Immunogenet.* **1:** 282–296.
31. Csencsits, K. L., and Bishop, D. K. (2003). Contrasting alloreactive CD4$^+$ and CD8$^+$ T cells: there's more to it than MHC restriction. *Am. J. Transplant* **3:** 107–115.
32. Miyoshi, H., Smith, K. A., Mosier, D. E., Verma, I. M., and Torbett, B. E. (1999). Transduction of human CD34$^+$ cells that mediate long-term engraftment of NOD/SCID mice by HIV vectors. *Science* **283:** 682–686.
33. Yahata, T., *et al.* (2003). A highly sensitive strategy for SCID-repopulating cell assay by direct injection of primitive human hematopoietic cells into NOD/SCID mice bone marrow. *Blood* **101:** 2905–2913.

ELSEVIER

Journal of Neuroimmunology 151 (2004) 189–194

Journal of Neuroimmunology

www.elsevier.com/locate/jneuroim

Short communication

Th1/Th2 balance and HTLV-I proviral load in HAM/TSP patients treated with interferon-α

Juan Feng[a], Tatsuro Misu[a], Kazuo Fujihara[a,*], Naoko Misawa[b], Yoshio Koyanagi[b], Yusei Shiga[a], Atsushi Takeda[a], Shigeru Sato[c], Sadao Takase[c], Takeshi Kohnosu[d], Hiroshi Saito[d], Yasuto Itoyama[a]

[a] *Department of Neurology, Tohoku University School of Medicine 1-1 Seiryomachi, Aobaku, Sendai 980-8574, Japan*
[b] *Department of Microbiology, Tohoku University School of Medicine, Japan*
[c] *Department of Neurology, Kohnan Hospital, Japan*
[d] *Department of Neurology, National Nishitaga Hospital, Japan*

Received 6 October 2003; received in revised form 15 January 2004; accepted 20 February 2004

Abstract

We studied the immunological and virological effects of interferon-α (IFN-α) therapy in nine patients with HTLV-I-associated myelopathy (HAM/TSP). After therapy, the percentages of CCR5+ cells in CD4+ cells significantly decreased in the cerebrospinal fluid as well as blood. The therapy also significantly lowered the intracellular IFN-γ+/interleukin-4+ T-cell ratio in blood. Those helper T-cell type 1 (Th1)-related responses tended to be higher and reduce more evidently following therapy in three patients who clinically improved. Also, all the three patients had one or more HTLV-I copies in five blood mononuclear cells. These results suggest that IFN-α suppresses Th1 responses in HAM/TSP and that the patients with higher Th1 immunity and proviral loads may be responders of the therapy. Larger-scale studies are needed to confirm the findings.

Keywords: HAM/TSP; HTLV-I; Interferon-alpha therapy; Helper T cell; Chemokine receptor

1. Introduction

Human T-lymphotropic virus type I (HTLV-I) is associated with chronic inflammatory myelopathy, HTLV-I-associated myelopathy/tropical spastic paraparesis (HAM/TSP) (Gessain et al., 1985; Osame et al., 1986; Izumo et al., 2000). Previous studies demonstrated remarkable immune activation including helper T-cell type 1 (Th1)-associated responses (Kuroda and Matsui, 1993; Itoyama et al., 1996; Umehara et al., 1994; Jacobson et al., 1998) and high HTLV-I proviral loads (Nagai et al., 1998) in HAM/TSP. These immunological and virological changes are probably important in the pathogenesis of this myelopathy and effective immunotherapies for HAM/TSP need to suppress these abnormalities.

A randomized, double-blind study demonstrated that interferon-α (IFN-α) was clinically effective in HAM/TSP (Izumo et al., 1996). The immunological effects of the therapy had been unclear, but we recently found a significant reduction of CD4 cell subsets in the cerebrospinal fluid (CSF) of the patients receiving the therapy (Feng et al., 2003). Here, we report Th1 and Th2-associated chemokine receptor expression on T cells, intracellular cytokine levels in T cells and HTLV-I proviral loads in blood before and after the therapy in the same patients.

2. Materials and methods

2.1. Subjects

Nine patients (five women and four men) were enrolled in the present study as reported previously (Feng et al., 2003). Their ages ranged from 54 to 72 years old and the duration of disease was from 2 to 50 years. The clinical disability was graded according to the Osame's scale: motor

* Corresponding author. Tel.: +81-22-717-7189; fax: +81-22-717-7192.
E-mail address: fujikazu@em.neurol.med.tohoku.ac.jp (K. Fujihara).

0165-5728/$ - see front matter © 2004 Elsevier B.V. All rights reserved.
doi:10.1016/j.jneuroim.2004.02.007

disability: grade 0 (normal)–13 (bedridden), dysuria: grade 0 (normal)–3 (severe) (Izumo et al., 1996). The patients received intramuscular injections of IFN-α (3 million units) daily for 4 weeks (Izumo et al., 1996). None had received immunosuppressants for the last 3 months except for a single patient (HAM3) who was treated with a fixed dose of oral prednisolone (20 mg/day) throughout the therapy. Age- and sex-matched nine HTLV-I-seronegative control subjects were studied for peripheral blood mononuclear cells (PBMC). We obtained informed consents prior to the study and the present study conformed to the guidelines of Medical Ethics Committee of our medical school.

2.2. Mononuclear cell preparation

Heparinized venous blood and CSF were collected before the IFN-α therapy and the next day of the last IFN-α injection. PBMC were isolated by Ficoll-Paque and CSF cells were directly isolated by centrifugation.

2.3. Flow cytometric analysis

2.3.1. T-cell subset

We analyzed T-cell subsets using a standard direct immunofluorescent technique with monoclonal antibodies (MoAbs), a three-color flow cytometer (FACSCalibur, Becton Dickinson, San Jose, CA) and the CellQuest software.

The analyzed subsets were CCR5+ and CXCR3+ (helper T-cell type 1 [Th1]-associated chemokine receptor expressing cells) and CCR3+ (Th2-associated chemokine receptor expressing cells, especially in the early stage of Th2 response) among CD4+ and CD8+ cells. Peridinin chlorophyll protein-conjugated anti-CD4 and anti-CD8, fluorescein isothiocyanate-conjugated anti-CD8 MoAbs were provided by Becton Dickinson. Phycoerythrin-conjugated anti-CCR5 and anti-CCR3 and carboxy-fluorescein succinimidylester-conjugated anti-CXCR3 MoAbs were purchased from Dako (Tokyo, Japan).

The data were expressed as the percentages of T-cell subsets in CD4+ or CD8+ cells.

2.3.2. Intracellular Th1/Th2-associated cytokines

The ratio of IFN-γ producing cells to interleukin-4 (IL-4) producing cells in CD3+ cells was assayed with a FACSCalibur according to the previous report (Pala et al., 2000).

2.4. HTLV-I proviral load in PBMC

DNA was extracted from PBMC. The HTLV-I proviral load was quantified using a real-time Taq-Man PCR method (PE Applied Biosystems, Foster City, CA). Standard curves of β-actin and HTLV-I tax genes were generated using DNA derived from an HTLV-I infected cell line, TloM1. TaqMan amplifications were carried out with the forward primers 5′-ACTCCTCAAGCGAGCTGCAT-3′, the reverse primer 5′-TTTTTCTTTGGGATCGGCG-3′ (Greiner Japan, Tokyo, Japan) and HTLV-I TaqMan Probe 5′-CCCAAGACCC-GTCGGAGGCC-3′ labeled with the 5′ FAM reporter dye and the 3′ TAMRA quencher dye molecules (Japan BioService, Asaka, Japan). The primers and probe for β-actin gene were obtained from PE Applied Biosystems. The thermal cycle conditions were 50 °C for 2 min followed by 95 °C for 10 min (hot start) and then 40 cycles were run by melting at 95 °C for 15 s and annealing/extension at 60 °C for 1 min in each cycle. Each sample was analyzed in triplicate. For each reaction, 100 ng of DNA, the equivalent of 2×10^4 cells, were subjected to the analysis. The amplifications were performed on an ABI PRISM 7700 sequence detector equipped with a 96-well thermal cycler. Copy numbers were reported as copy equivalents per 10^5 PBMC.

2.5. Statistical analysis

We used Mann–Whitney *U*-test to compare the unpaired values, Wilcoxon's signed rank test to compare the paired values. We also examined correlations in clinical disability, immunological and virological parameters (motor disability grade, percentages of CCR5+, CXCR3+ and CCR3+ in CD4+ cells, and CCR5+, CXCR3+ and CCR3+ in CD8+ cells in the CSF and blood, ratio of IFN-γ producing cells to IL-4 producing cells in blood CD3+ cells, and HTLV-I proviral load) of the HAM/TSP patients with Spearman rank correlation coefficient test. Correlations in both baseline values and the changes after the IFN-α therapy were analyzed. *P*-values less than 0.05 were considered statistically significant.

3. Results

3.1. Clinical effects

The motor disability grade improved in three patients after the IFN-α therapy (Patients HAM 3, grade 3 → 2; HAM 5, grade 8 → 6; HAM 6, grade 6 → 4) as we reported (Feng et al., 2003). The dysuria grade did not change.

3.2. T-cell subsets (Table 1)

3.2.1. CCR5

The percentage of CCR5+ cells in blood CD4+ cells was significantly higher before the IFN-α therapy in HAM/TSP than in control. In HAM/TSP, the mean percentages of all CCR5+ T-cell subsets in blood and CSF decreased after the therapy. Among them, the percentage of CCR5+ cells in blood CD4+ cells of HAM/TSP significantly decreased after the therapy, and they were no longer different between HSM/TSP and control. The percentage of CCR5+ cells in CSF CD4+ cells also significantly decreased after the therapy (Table 1).

Table 1
T cells expressing Th1/Th2-associated chemokine receptors in HAM/TSP patients treated with interferon-α and in control subjects

	CCR5+ in CD4+	CXCR3+ in CD4+	CCR3+ in CD4+
Control (n=9)	(%)	(%)	(%)
Blood	0.5 ± 0.1	27.3 ± 4.8	0.3 ± 0.1
HAM/TSP (n=9)			
Blood			
before IFN-α	1.5 ± 0.9 *	27.9 ± 12.3	0.3 ± 0.2
after IFN-α	0.9 ± 0.8 *	25.5 ± 7.6	0.4 ± 0.2
CSF			
before IFN-α	20.5 ± 8.8 *	88.5 ± 5.4	4.3 ± 4.3
after IFN-α	13.4 ± 5.3 *	81.3 ± 12.2	7.5 ± 3.1
	CCR5+ in CD8+	CXCR3+ in CD8+	CCR3+ in CD8+
Control (n=9)	(%)	(%)	(%)
Blood	0.9 ± 0.9	35.9 ± 8.1 *	0.5 ± 0.2
HAM/TSP (n=9)			
Blood			
before IFN-α	3.0 ± 4.5	55.5 ± 17.4 *	0.7 ± 0.4
after IFN-α	1.6 ± 1.0	36.4 ± 17.6 *	0.6 ± 0.2
CSF			
before IFN-α	27.1 ± 12.1	94.8 ± 4.4	4.3 ± 4.3
after IFN-α	17.9 ± 6.5	90.3 ± 9.3	7.5 ± 3.6

Data are mean percentages ± standard deviation.
*$P < 0.05$.

The percentage of CCR5+ cells in CSF CD4 cells was unequivocally higher in the three patients who clinically improved after the therapy (the lowest value was 26.8% in Patient HAM 6) than in the six patients without clinical effect (the highest value was 18.3% in Patient HAM 2).

3.2.2. CXCR3

In blood, the percentages of CXCR3+ cells in CD8+ cells were significantly higher in HAM/TSP before the therapy than in control. In HAM/TSP, the mean percentages of all CXCR3+ T-cell subsets in blood and CSF decreased after the therapy. Among them, the percentage of CXCR3+ cells in CD8+ cells significantly decreased after the therapy in HAM/TSP, and it was no longer different between HAM/TSP and control.

3.2.3. CCR3

No CCR3+ subset was significantly different between HAM/TSP and control or changed significantly after the therapy in HAM/TSP, although the mean percentages of CCR3+ cells in CSF CD4+ and CD8+ cells increased after the therapy.

3.3. Intracellular TH1/TH2-associated cytokines (Fig. 1)

The IFN-α therapy significantly decreased the ratio of intracellular IFN-γ- versus IL-4-producing T cells in blood (9.5 ± 7.6 before the therapy and 5.8 ± 4.9 after the therapy). The ratios in the three patients who clinically improved following the therapy (Patients HAM 3, 5 and 6) were over 5.0, while the therapy was not effective in any of the four patients with the ratios being less than 5.0 (Patients HAM 9, 4, 1 and 7).

3.4. HTLV-I proviral load (Fig. 2)

The HTLV-I proviral copy number before the IFN-α therapy in the nine patients was 13272 ± 9006 copies and

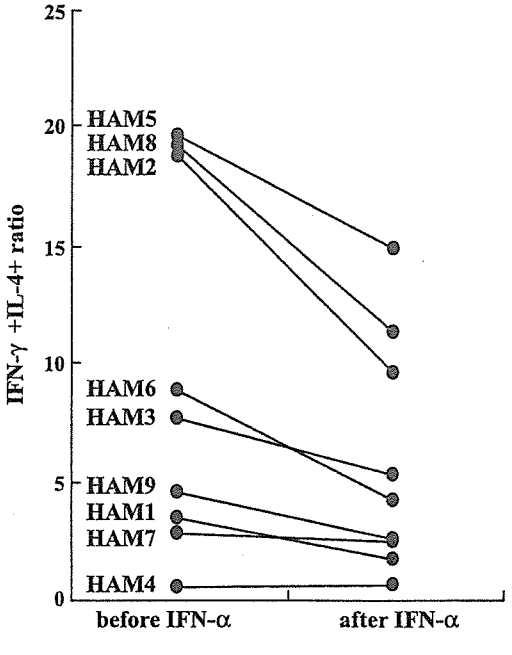

Fig. 1. Intracellular Th1/Th2 cytokine balance in T cells of the patients with HAM/TSP treated with IFN-α. The ratio of IFN-γ+ cells to IL-4+ cells among CD3+ T cells was significantly lower after the IFN-α therapy. Before-IFN-α, before IFN-α therapy; after-IFN-α, after IFN-α therapy.

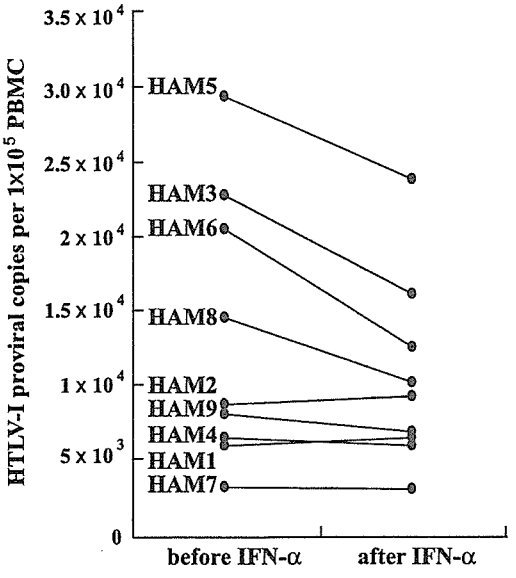

Fig. 2. HTLV-I proviral loads in the PBMC of the patients with HAM/TSP treated with IFN-α. After the IFN-α therapy, HTLV-I proviral loads apparently decreased in the patients with higher proviral loads, and clinical effect was seen in the three patients with 2×10^4 copies or more in 10^5 PBMC (HAM3, HAM5 and HAM6). Before-IFN-α, before IFN-α therapy; after-IFN-α, after IFN-α therapy.

that after the therapy was 10472 ± 6323 copies ($P = 0.06$). Patients HAM 3, 5, 8 and 6, who had the highest proviral loads and who experienced the most obvious decline in proviral load as a result of therapy, were among the ones with the highest baseline ratios of intracellular IFN-γ- versus IL-4-producing blood T cells and with the most dramatic decline in those values following the therapy (Fig. 1). Furthermore, three of these four patients were the ones who clinically improved, and all the three patients had 2×10^4 HTLV-I copies or more in 10^5 PBMC. Meanwhile, clinical effect was not seen in any patient with lower HTLV-I proviral load and their proviral loads remained unchanged after the therapy (Fig. 2).

3.5. Correlation

None of the correlations in clinical disability, immunological and virological parameters in the HAM/TSP patients was statistically significant.

3.6. Comparison of immunological and virological findings in responders and non-responders to IFN-α therapy

We compared the immunological and virological findings in responders (Patients HAM 3, 5 and 6) and non-responders (Patients HAM 1, 2, 4, 7, 8 and 9) to the IFN-α therapy (Table 2). We could not analyze the data statistically due to the small sample size. However, among the significant parameters in the statistical analyses of HAM/TSP patients, there was a tendency for the percentages of CCR5+ cells in CD4+ cells in the CSF and blood, the ratio of intracellular IFN-γ- versus IL-4-producing T cells in blood, and the HTLV-I proviral load to be higher and reduce more evidently following the therapy in responders as compared with non-responders. In the other parameters, the percen-

Table 2
Immunological and virological data in "responders" and "non-responders" to the interferon-α therapy

	CCR5+ in CD4+ (%)	CXCR3+ in CD4+ (%)	CCR3+ in CD4+ (%)	CCR5+ in CD8+ (%)	CXCR3+ in CD8+ (%)	CCR3+ in CD8+ (%)	IFN-γ/ IL-4 ratio	HTLV-1 proviral load (copies/10^5 PBMC)
Blood								
Responders								
(A) Before therapy	2.0 ± 1.1	28.7 ± 7.8	0.4 ± 0.1	5.6 ± 7.6	49.1 ± 21.2	0.5 ± 0.1	11.8 ± 6.1	24156 ± 4666
(B) After therapy	1.1 ± 0.3	23.3 ± 4.8	0.4 ± 0.2	2.1 ± 1.0	37.2 ± 17.4	0.6 ± 0.4	6.4 ± 2.9	17506 ± 5694
(A)–(B)	0.9 ± 0.4	6.4 ± 7.6	0.0 ± 0.1	3.5 ± 6.6	11.8 ± 4.0	0.1 ± 0.2	5.4 ± 3.5	6650 ± 1107
Non-responders								
(A) Before therapy	1.2 ± 0.8	26.1 ± 10.9	0.4 ± 0.1	1.7 ± 1.7	51.2 ± 19.0	0.8 ± 0.5	8.3 ± 8.7	7830 ± 3802
(B) After therapy	1.0 ± 1.0	26.0 ± 8.8	0.4 ± 0.1	1.3 ± 1.0	37.4 ± 17.6	0.5 ± 0.1	5.6 ± 5.9	6954 ± 2538
(A)–(B)	0.4 ± 0.2	2.4 ± 3.2	0.1 ± 0.2	0.5 ± 0.0	13.8 ± 10.1	0.2 ± 0.5	2.7 ± 3.0	876 ± 1851
CSF								
Responders								
(A) Before therapy	33.5 ± 9.0	92.7 ± 0.8	8.8 ± 5.7	35.4 ± 17.1	97.8 ± 3.1	6.1 ± 2.8		
(B) After therapy	19.4 ± 3.0	89.5 ± 3.2	9.0 ± 4.6	25.4 ± 19.7	96.8 ± 0.5	7.5 ± 1.4		
(A)–(B)	14.1 ± 5.9	3.1 ± 4.0	−0.2 ± 1.1	9.9 ± 19.0	1.0 ± 2.6	−1.5 ± 1.3		
Non-responders								
(A) Before therapy	15.3 ± 2.0	86.8 ± 5.6	2.1 ± 0.6	23.9 ± 9.9	93.6 ± 4.5	3.1 ± 2.9		
(B) After therapy	10.9 ± 4.0	78.0 ± 13.2	6.1 ± 0.2	15.9 ± 5.3	87.9 ± 9.0	7.6 ± 5.0		
(A)–(B)	4.2 ± 2.4	8.8 ± 17.4	−4.5 ± 0.4	8.9 ± 12.2	5.8 ± 11.2	−4.8 ± 6.2		

Data are shown as mean ± standard deviation.
IFN-γ, interferon-gamma; IL-4, interleukin-4; IFN-γ/IL-4, ratio of IFN-γ producing cells to IL-4 producing cells in CD3+ cells; PBMC, peripheral blood mononuclear cells; CSF, cerebrospinal fluid.

tages of CCR3+ cells in CSF CD4+ and CD8+ cells tended to be lower and increase more after the therapy in non-responders than in responders.

4. Discussion

Our previous analysis revealed a significant reduction of CD4+ cells in CSF of HAM/TSP after IFN-α therapy (Feng et al., 2003). In the present study, we focused on the Th1/Th2 balance and showed that IFN-α therapy significantly reduced CCR5 + CD4+ cells, a Th1 subset, in the patients' CSF as well as blood. The CCR5 + CD4+ cell subset in CSF reflects the disease activity in multiple sclerosis (Misu et al., 2001). This subset is increased in the synovium of active rheumatoid arthritis (Mack et al., 1999), and the inhibition of CCR5 successfully treated adjuvant arthritis in rats, an animal model of rheumatoid arthritis (Barnes et al., 1998). In HAM/TSP, elevated levels of CCR5 on memory CD4+ cells in PBMC (Wu et al., 2000) and macrophage inflammatory protein-1α, a CCR5 ligand, in CSF (Miyagishi et al., 1995) were reported. These findings suggest a pathogenic role of CCR5 + CD4+ cells in HAM/TSP and other immunologic diseases, and a suppression of the subset by IFN-α might relate to the alleviation of myelitis in HAM/TSP.

There was also a tendency for the CXCR3 + CD4 cell, another Th1 subset, to be decreased and CCR3 + CD4+ cells, a Th2 subset, to be increased in CSF of the treated patients. A significant decrease in blood CD8+ cell number in the treated patients (Feng et al., 2003) may be attributable to the reduction in CXCR3 + CD8+ cells. Moreover, intracellular Th1/Th2-associated cytokine ratio in T cells, which was analyzed only in blood because of the limited volumes of CSF, reduced significantly following the therapy. Taken together, our data suggests that the IFN-α therapy suppressed Th1-related responses in HAM/TSP, although our small-scale study did not address whether the immunological changes were directly associated with the clinical efficacy of IFN-α in HAMTSP.

The present study suggested some interesting differences in baseline immunological and virological findings between responders and non-responders to the IFN-α therapy, that is, responders showed higher Th1 responses and more viral replication than non-responders, and the therapeutic suppression to those parameters was more evident in responders. Our small-scale study could not confirm the associations statistically, but those analyses will be critically important to reliably predict therapeutic efficacy of intramuscular injections of IFN-α beforehand. Whether such laboratory data as (1) baseline percentage of CCR5+ cells in CSF CD4+ cells >20%, (2) baseline ratio of intracellular IFN-γ- versus IL-4-producing blood T cells >5.0 and (3) baseline HTLV-I proviral load more than one copy in five PBMC are really linked to clinical efficacy of IFN-α therapy in HAM/TSP need to be examined in a larger cohort of patients by statistical analyses.

Acknowledgements

The authors thank Mr. Brent Bell for reading the manuscript. This work was supported by the grants from the Ministry of Education, Science, Culture, Sports and Technology and the Tawara's Endowment for HAM Research.

References

Barnes, D.A., Tse, J., Kaufhold, M., Owen, M., Hesselgesser, J., Strieter, R., Horuk, R., Perez, H.D., 1998. Polyclonal antibody directed against human RANTES ameliorates disease in the Lewis rat adjuvant-induced arthritis model. J. Clin. Invest. 101, 2910–2919.

Feng, J., Misu, T., Fujihara, K., Saito, H., Takahashi, T., Kohnosu, T., Shiga, Y., Takeda, A., Sato, S., Takase, S., Itoyama, Y., 2003. Interferon-alpha significantly reduces cerebrospinal fluid CD4 cell subsets in HAM/TSP. J. Neuroimmunol. 141, 170–173.

Gessain, A., Barin, F., Vernant, J.C., Gout, O., Maurs, L., Calender, A., de The, G., 1985. Antibodies to human T-lymphotropic virus type-I in patients with tropical spastic paraparesis. Lancet 2, 407–410.

Itoyama, Y., Kira, J., Fujii, N., Goto, I., Yamamoto, N., 1996. Increases in helper inducer T cells and activated T cells in HTLV-I-associated myelopathy. Ann. Neurol. 26, 257–262.

Izumo, S., Goto, I., Itoyama, Y., Okajima, T., Watanabe, S., Kuroda, Y., Araki, S., Mori, M., Nagataki, S., Matsukura, S., Akamine, T., Nakagawa, M., Yamamoto, I., Osame, M., 1996. Interferon-alpha is effective in HTLV-I-associated myelopathy: a multicenter, randomized, double-blind, control trial. Neurology 46, 1016–1021.

Izumo, S., Umehara, F., Osame, M., 2000. HTLV-I-associated myelopathy. Neuropathology 20, S65–68 (Suppl).

Jacobson, S., Levin, M., Utz, U., Drew, P., 1998. Infectious immune disorders: HTLV-I. In: Antel, J.P., Birnbaum, G., Hartung, H.P. (Eds.), Clinical neuroimmunology. Blackwell, Malden, pp. 204–217.

Kuroda, Y., Matsui, M., 1993. Cerebrospinal fluid interferon-gamma is increased in HTLV-I-associated myelopathy. J. Neuroimmunol. 42, 223–236.

Mack, M., Bruhl, H., Gruber, R., Jaeger, C., Cihak, J., Eiter, V., Plachy, J., Stangassinger, M., Uhlig, K., Schattenkirchner, M., Schlondorff, D., 1999. Predominance of mononuclear cells expressing the chemokine receptor CCR5 in synovial effusions of patients with different forms of arthritis. Arthritis Rheum. 42, 981–988.

Misu, T., Onodera, H., Fujihara, K., Matsushima, K., Yoshie, O., Okita, N., Takase, S., Itoyama, Y., 2001. Chemokine receptor expression on T cells in blood and cerebrospinal fluid at relapse and remission of multiple sclerosis: imbalance of Th1/Th2-associated chemokine signaling. J. Neuroimmunol. 114, 207–212.

Miyagishi, R., Kikuchi, S., Fukazawa, T., Tashiro, K., 1995. Macrophage inflammatory protein-1 alpha in the cerebrospinal fluid of patients with multiple sclerosis and other inflammatory neurological diseases. J. Neurol. Sci. 129, 223–227.

Nagai, M., Usuku, K., Matsumoto, W., Kodama, D., Takenouchi, N., Moritoyo, T., Hashiguchi, S., Ichinose, M., Bangham, C.R., Izumo, S., Osame, M., 1998. Analysis of HTLV-I proviral load in 202 HAM/TSP patients and 243 asymptomatic HTLV-I carriers: high proviral load strongly predisposes to HAM/TSP. J. Neurovirol. 4, 586–593.

Osame, M., Usuku, K., Izumo, S., Ijichi, N., Amitani, H., Igata, A., Matsumoto, M., Tara, M., 1986. HTLV-I associated myelopathy, a new clinical entity. Lancet 1, 1031–1032.

Pala, P., Hussell, T., Openshaw, P.J., 2000. Flow cytometric measurement of intracellular cytokines. J. Immunol. Methods 243, 107–124.

Umehara, F., Izumo, S., Ronquillo, A.T., Matsumuro, K., Sato, E.,

Osame, M., 1994. Cytokine expression in the spinal cord lesions in HTLV-I-associated myelopathy. J. Neuropathol. Exp. Neurol. 53, 72–77.

Wu, X.M., Osoegawa, M., Yamasaki, K., Kawano, Y., Ochi, H., Horiuchi, I., Minohara, M., Ohyagi, Y., Yamada, T., Kira, J.I., 2000. Flow cytometric differentiation of Asian and Western types of multiple sclerosis, HTLV-I-associated myelopathy/tropical spastic paraparesis (HAM/TSP) and hyperIgEaemic myelitis by analyses of memory CD4 positive T cell subsets and NK subsets. J. Neurol. Sci. 177, 24–31.

Available online at www.sciencedirect.com
SCIENCE DIRECT
Microbes and Infection 6 (2004) 715–724
Microbes and Infection
www.elsevier.com/locate/micinf

Original article

Role of Nup98 in nuclear entry of human immunodeficiency virus type 1 cDNA

Hirotaka Ebina [a], Jun Aoki [a], Shunsuke Hatta [a], Takeshi Yoshida [a], Yoshio Koyanagi [b,*]

[a] *Department of Virology, Tohoku University Graduate School of Medicine, Sendai 980-8575, Japan*
[b] *Laboratory of Viral Pathogenesis, Institute for Virus Research, Kyoto University, 53 Shougoin-kawahara machi, Sakyou-ku, Kyoto 606-8507, Japan*

Received 18 February 2004; accepted 7 April 2004

Available online 24 May 2004

Abstract

Human immunodeficiency virus type 1 (HIV-1), like other lentiviruses, can infect non-dividing cells. The lentiviruses are most likely to have evolved a nuclear import strategy to import HIV-1 cDNA and viral protein complex through the nuclear pore complex (NPC) formed by nucleoporin proteins (Nup). In this study, we found that synthesis of integrated and 2LTR but not full-length form of HIV-1 cDNA was clearly impaired in culture via transduction of vesicular stomatitis virus matrix protein (VSV M), an inhibitor protein, through binding to the phenylalanine-glycine (FG) repeat region of Nup98. The impairment of synthesis of integrated and 2LTR DNA with VSV M was restored by ectopic overexpression of Nup98. A series of experiments using Nup98-depleted NPC by the small interfering RNA (siRNA) technique showed specific impairment of NPC structure and some functions, including nuclear import of HIV-1 cDNA. Our results suggest that Nup98 on the NPC specifically participates in the nuclear entry of HIV-1 cDNA following HIV-1 entry.

Keywords: Nucleoporin; NPC; HIV-1; Nuclear import

1. Introduction

The Retroviridae family of viruses can reverse transcribe their RNA genome into cDNA and then integrate the cDNA into host chromosomes. The lentiviruses (e.g. HIV) are distinguished by their ability to infect non-dividing cells, whereas the gamma-retroviruses (e.g. Moloney murine leukemia virus) require nuclear membrane dissolution to access the host cell DNA [1]. Thus, the lentiviruses are most likely to have evolved a nuclear import strategy, which allows their cDNA to cross the nuclear membrane independently of mitosis. In the case of human immunodeficiency virus type 1 (HIV-1), mitosis-independent replication was initially shown in terminally differentiated macrophages in vitro [1–3]. The mitosis-independent replication of HIV has also enabled the generation of integration-competent gene transfer vectors with promising therapeutic applications in a variety of non-dividing cellular hosts, including neurons [4], myocytes [5], and retinal cells [6]. To facilitate integration into a host DNA, a preintegration complex (PIC) is generated in the cytoplasm immediately after completion of reverse transcription. The PIC can be isolated successfully from in vitro freshly HIV-1-infected or HIV vector-infected cells and was recently shown to have the ability to traverse the nuclear pore complex (NPC) [1,7]. The NPCs serve as the conduits for bi-directional transport of macromolecules. Translocation across the NPC into the nucleus and from the nucleus into the cytoplasm is governed by a class of proteins known as importins and exportins (transport receptors), respectively. Both are members of the karyopherin family. The transport receptors engage the appropriate import or export signals and mediate their transport [8,9]. The PIC contains a double-strand linear cDNA as well as at least four viral proteins: matrix (MA), reverse transcriptase (RT), integrase (IN), and viral protein R (VPR), and has a diameter of approximately 56 nm, which greatly exceeds the 25 nm central channel of the NPC [1,7,10]. The NPC has a large supramolecular structure formed of ~50 unique proteins in eukaryotic cells, termed nucleoporins (Nup) [8,9,11,12]. High-resolution electron microscopic images of NPCs reveal an eightfold

* Corresponding author. Tel.: +81-75-751-4811; fax: +81-75-751-4812.
E-mail address: ykoyanag@virus.kyoto-u.ac.jp (Y. Koyanagi).

doi:10.1016/j.micinf.2004.04.002

symmetric structure, formed by nuclear and cytoplasmic rings and central spoke complex. The Nups often contain multiple phenylalanine-glycine (FG) dipeptide repeats clustered in domains, which in vertebrates are glycosylated by addition of *O*-linked *N*-acetylglucosamine (GlcNAc). Some of these Nups are localized asymmetrically at the NPC [9,11]. The asymmetric distribution of nucleoporins and the different affinities for import and export complexes may be important in determining the direction of transport [13,14]. Recent studies reported that importin 7 is involved in the nuclear entry of HIV-1 PIC as one of the main transport receptors [15]. However, the steps involved in the NPC remain largely undefined. In the present study, we show that nuclear import of HIV-1 cDNA requires NPC, and Nup98 has a role in nuclear entry of HIV-1 cDNA.

2. Materials and methods

2.1. Chemical treatment

Aphidicolin (APH) (Sigma Chemical Co., St. Louis, MO, USA), actinomycin D (ActD) (Sigma), zidovudine (AZT) (Sigma) or leptomycine B (LMB) (Sigma) was used. APH treatment (5 μg/ml) started 24 h before HIV-1 vector infection. AZT treatment started at the time of infection. LMB was added 2 h after infection. ActD was added 5 h after infection. DNA was extracted 24 h after infection.

2.2. Transfection

Human 293T cells were maintained in D-MEM containing 10% fetal calf serum (FCS). 293T cells were transfected with vesicular stomatitis virus matrix protein (VSV M)-, Nup98- or small interfering RNA (siRNA)-expressing DNA using calcium phosphate methods.

2.3. Quantitative polymerase chain reaction (PCR) assay

For the detection and quantification of individual forms of HIV-1 DNA, full-length/1LTR circle, 2LTR circle and integrated forms, we used a set of primer pairs and fluorogenic probes, as described previously [16,17]. PCR was performed using an ABI PRISM 7700 sequence detection system (PE-Applied Biosystems, Foster City, CA, USA) and TaqMan Universal PCR Master Mix (PE-Applied Biosystems). Cycling conditions included a hot start (50 °C for 2 min, 95 °C for 10 min), followed by 40 cycles of denaturation (95 °C for 15 s) and extension (60 °C for 1 min). To measure the integrated DNA, an *Alu*-sequence-specific sense primer and an antisense HIV-specific primer were used in the first PCR and subsequently 1000-fold diluted products were subjected to real-time PCR assay for measurement of R/U5 DNA, as described previously [16,17].

2.4. Cell-cycle analysis

Cell-cycle progression was examined by single-color flow cytometric analysis of the DNA content stained with 50 μg/ml of propidium iodine (Sigma).

2.5. DNA constructs and recombinant protein expression

Small interference RNA (siRNA)-expressing plasmid DNAs were constructed using the method described by Miyagishi and Taira [18]. The sequences inserted in the *Bfu*AI site of pU6i cassette, immediately downstream of the U6 promoter, were as follows: Nup98-targeted siRNA (siN98), 5′-CACC**GAATATGAAAG*T*AAGTT*A*TTA**TAGAATTACATCAAGGGAGAT**TAGTGACTTGCTTTCATATTC**TTTTTATGC-3′; firefly luciferase-targeted siRNA (siLuc), 5′-CACC**GTGCG*T*TG*T*TGGTG*TT*AA*T*CC**ATCTCCCTTGATGTAATTCTA**GGGTTGGCACCAGCAGCGCAC**TTTTTATGC-3′. Bold-lettered nucleotides are the siRNA sequences, italic nucleotides are mutated, and underlined nucleotides are loop sequences. The siRNA-expressing DNA fragment was also inserted into the *Eco*RI site of a lentivirus vector DNA, pCS-CDF-EH2K^k, and an enhanced green fluorescence protein (EGFP) fragment between the *Age*I and *Xho*I sites of pCS-CDF-EG-PRE [19] was replaced with a H-2K^k fragment (Daiichi pure chemicals, Tokyo, Japan).

HA-tagged human Nup98-expressing plasmid DNA (p37R-HANup98) and EGFP-fused VSV M-expressing DNA (pEGFPN3-M) [20] were kindly provided by Dr. Elisa Izaurralde (European Molecular Biology Laboratory). A *Bss*HII-*Xho*I DNA fragment covering the coding region of HA-tagged human Nup98 region was cloned into a site downstream of CMV promoter in pcDNA3.1/Zeo (+) (Invitrogen, Carlsbad, CA, USA) (pcDNup98). Alanine substitutions from Asp-Thr-Tyr at the position of VSV M 52–54 [VSV (M)] were introduced using an oligonucleotide-directed in vitro mutagenesis system (Quickchange site-directed mutagenesis, Stratagene, San Diego, CA, USA). DsRed-fusion recombinant protein with NLS, U1A and rpL23a was produced in *Escherichia coli*. A double-strand synthetic nucleotide of SV40 NLS (5′-CCA TGC ATA TGC CAA AAA AGA AGA GAA AGG TTG-3′) and PCR-amplified DNA fragment of U1A (1–486), or rpL23a (1–486) from mRNA of HeLa cells was cloned into the *Sma*I or *Sal*I-*Bam*HI sites of pDsRed1-N1 (Clontech, Palo Alto, CA, USA), and then a *Sal*I-*Not*I fragment was inserted in the *Sal*I-*Not*I site of pGEX-4T-2 (Amersham Pharmacia Biotech, Piscataway, NJ, USA). *E. coli* ER2566 (New England Biolabs Inc., Beverly, MA, USA) was used, and recombinant proteins were purified on glutathione sepharose 4 Fast Flow (Amersham) by standard protocols, as previously described [21].

2.6. Reverse-transcription PCR

Total RNA was extracted from transiently transfected cells by using a RNeasy RNA-preparation Kit (Qiagen, KJ

Venlo, The Netherlands). Reverse transcription and PCR were carried out using a SuperScript One-Step RT-PCR with Platinum Taq (Invitrogen). We used the following primers to detect the specific transcripts: for Nup107, 5′-AAACGCG-GTAGCTAAACTGCA-3′, 5′-ACCACCAGCTGACTT-TGTCGA-3′; for Nup214, 5′-CTTGCCACGAAAAC-CGTGA-3′, 5′-CAACCCGCAGTCCTGAAAA-3′; for p62, 5′-CAGACACCGACGGATTTGCTT-3′, 5′-TGGATGTTG-TTGTGGAGGTGC-3′; for Nup98, 5′-TCTCATCCCAA-AACAATGCCTT-3′, 5′-AAACAAAGATGCCTGTCC-AGCA-3′; for Nup153, 5′-TGACAATGAAGAGCC-AAAGTGT-3′, 5′-TAGGAGTTGTTCCAGAGCCAAA-3′. TaqMan GAPDH Control Reagents (PE-Applied Biosystems) were used as primer sets for glyceraldehyde 3-phosphate dehydrogenase (GAPDH). Fifty nanograms of template RNA and 10 pmol of specific primers were used. The efficiency of PCR amplification was roughly in the linear range, as determined by preliminary test with increasing number of cycles. Finally, the PCR products were analyzed by agarose gel electrophoresis using standard techniques.

2.7. Virus vector infection

For HIV-1 vector preparation, a replication-incompetent EGFP-expressing lentivirus (pCS-CDF-CG-PRE) or siRNA-expressing lentivirus was co-transfected into 293T cells along with VSV G-expressing plasmid (pVSV G), HIV-Gag-Pol-expressing plasmid (pRRE) and Rev-expressing plasmid (pRSV-Rev) as described before [6,19]. Three days after transfection, the culture supernatants were cleared by filtration and concentrated through centrifugation at 6000 × *g* for 16 h at 4 °C. The transducing unit (TU) was determined by measurement of EGFP-, or H-2K^k-expressing cells using flow cytometry. Phycoerythrin-labeled anti-mouse H-2K^k monoclonal antibody (mAb) (Cedarlane, Ontario, Canada) was used. Cells were analyzed on FACS SCAN, using Cell Quest software (BD PharMingen, San Diego, CA, USA). Treatment with DNaseI (20 μg/ml) was performed to remove plasmid DNA in the virus stocks. Heat-inactivated (65 °C, 30 min) virus liquid was used as negative control for HIV DNA quantification in infected cells. APH-treated MT-2 cells or 293T cells (2×10^5 cells) were infected with HIV-1 vector (4×10^5 TU). Two hundred thousand 293T cells were transfected with VSV M- or Nup98-expressing DNA and then 24 h later, infected with HIV-1 vector (4×10^5 TU). Two hundred thousand 293T cells were transfected with siRNA-expressing DNA and then 72 h later, infected with HIV-1 vector (4×10^5 TU). The amount of viral DNA was measured by the quantitative PCR assay 24 h after infection, as described above. HeLa cells (1×10^5 cells), grown on cover-slips, were infected with siRNA-expressing HIV-1 vector at multiplicity of infection (m.o.i.) of 1. The cells were analyzed 96 h later by immunofluorescence, immunoblotting or nuclear import assay.

2.8. Immunofluorescence analysis

HeLa cells, grown on cover-slips, were washed twice with phosphate-buffered solution (PBS) and fixed in 4% (vol/vol) paraformaldehyde/PBS for 15 min at room temperature. The cells were permeabilized with 0.2% Triton X-100/PBS for 5 min. After blocking with 5% bovine serum albumin (BSA)/0.1% Triton X/PBS for 1 h, the cells were incubated with an NPC-specific mouse mAb, mAb414 (BabCO, Berkeley, CA, USA) or anti-Nup98 polyclonal antibody (C-16) (Santa Cruz Biotechnology Inc., Santa Cruz, CA, USA) at 4 °C overnight. Cells were washed three times with 0.05% Triton X/PBS and then incubated with Alexa 594-conjugated goat anti-mouse IgG antibody (Molecular Probes, Eugene, OR, USA) or fluorescein isothiocyanate (FITC)-conjugated donkey anti-goat IgG antibodies (Chemicon, Temecula, CA, USA) for 1 h. Cells were washed three times with 0.05% Triton X/PBS, mounted in Vectashield mounting medium for fluorescence (Vector Laboratories, Burlingame, CA, USA) and analyzed with a Leica QFluoro system. The cells were also stained with Hoechst 33342 (Molecular Probes).

2.9. Nuclear import assay

HeLa cells grown on cover-slips were washed in PBS and permeabilized for 5 min on ice in 50 μg/ml digitonin (Sigma)/transport buffer (20 mM Hepes– NaOH, pH 7.3, 110 mM CH_3COOK, 2 mM $(CH_3COO)_2Mg$, 5 mM CH_3COONa, and 2 mM dithiothreitol). After washing three times with transport buffer, cells were incubated at 30 °C for 30 min in the presence of energy-regenerating system (1 mM ATP, 1 mM GTP, 10 mM creatine phosphate, and 20 U/ml creatine phosphokinase), 3 μM DsRed-labeled recombinant protein, and cytoplasmic extract from 2×10^5 HeLa cells. Samples were washed three times in transport buffer, fixed on ice for 30 min with 1% formalin/transport buffer and analyzed with a Leica QFluoro system.

2.10. Immunoblotting

293T cells were co-transfected with an HA-tagged human Nup98-expressing plasmid DNA (pcDNup98) and a siRNA-expressing plasmid (siN98 or siLuc). Three days after transfection, the cells were washed twice and lysed in RIPA buffer (0.5% NP-40 in 20 mM Tris–HCl [pH 8.2], 0.15 M NaCl, 5 mM iodoacetamide, and 1 mM phenylmethylsulfonyl fluoride). After loading on SDS/PAGE, polypeptides were transferred to Immobilion Transfer Membranes (Millipore, Billerica, MA, USA), the level of Nup98 was determined using a goat anti-Nup98 polyclonal antibody (C-16), biotin-conjugated rabbit anti-goat IgG (Chemicon) and then incubated with horseradish peroxidase (HRP)-conjugated streptavidin (Zymed, San Francisco, CA, USA). The filter generated from HeLa cells infected with siRNA-expressing

HIV-1 vector as described above was also incubated with mAb414 (mainly reactive against p62), biotin-conjugated horse anti-mouse IgG (VECTOR) and HRP-conjugated streptavidin. The specific bands were detected using Western Lighting Chemiluminescence Reagent (Perkin–Elmer Life Science, Boston, MA, USA). For detection of Nup98-VSV M complex, 293T cells were co-transfected with Nup98-expressing plasmids (pcDNup98) and EGFP-fused VSV M-expressing plasmid DNA (pEGFPN3-M) or the mutant [VSV M(D)]. Two days after transfection, the cells were lysed in triple detergent lysis buffer (1% NP-40, 0.1% SDS, 0.5% sodium deoxycholate in 50 mM Tris–HCl [pH 8.0], 0.15 M NaCl, 1 μg/ml aprotinin, 1 mM phenylmethylsulfonyl fluoride), and a mouse anti-HA mAb (F-7) (Santa Cruz) was added. After incubation for 12 h at 4 °C with protein G-sepharose (Amersham), the precipitate was washed three times with triple detergent lysis buffer, and the bound proteins were eluted by 1× sample buffer (1.71% SDS in 175 mM Tris–HCl [pH 6.8], 5% glycerol, 1% 2-mercaptoethanol) at 37 °C for 30 min. The samples were loaded on SDS/PAGE and transferred to Immobilon Transfer Membranes. For detection of the Nup98, a goat anti-Nup98 polyclonal antibody (C-16) (Santa Cruz) and biotin-conjugated rabbit anti-goat IgG (Chemicon) were used. For detection of VSV M, a rabbit anti-GFP polyclonal antibody (Santa Cruz) and biotin-conjugated donkey anti-rabbit IgG (Chemicon) were used.

2.11. Statistical analysis

All data were expressed as mean ± standard deviations (S.D.). Differences between groups were examined for statistical significance using the Welch's *t*-test. A P value less than 0.05 denoted the presence of a statistically significant difference.

3. Results

3.1. Efficient nuclear import of HIV-1 cDNA in infected cells

It has been shown that HIV and HIV-based lentivirus vectors efficiently infect non-dividing cells [2,6]. To determine the integration efficiency in dividing and non-dividing cells, we prepared cell-cycle-arrested T cell culture using MT-2 cells treated with APH, an inhibitor of DNA polymerase α. Under this condition, cell-cycle was confirmed to be stopped at G1 phase from flow cytometric analysis (Fig. 1A). The same numbers of treated (arrested) or untreated (proliferating) cells were infected with the same amounts of HIV-1 vector and the arrested culture was further maintained in the presence of APH. Since in this experiment we used a single-round infection system, we could estimate the precise efficiency of reverse transcription, nuclear translocation as well as integration. Total DNA was extracted 24 h after infection and a set of real-time PCR assay was performed [16,17]. Using this assay, we were able to measure the full-length/1LTR circle, 2LTR circle and integrated forms of HIV-1 cDNA, respectively. Since the 2LTR circle and integrated forms are found only in nucleus after HIV infection [3,22], we could estimate the efficiency of nuclear entry as well as integration of HIV-1 cDNA. Fig. 1B shows that the levels of integrated, 2LTR and full-length/1LTR circle form in proliferating cultures were higher than those in arrested cultures, because the numbers of the cells were two to three times greater in proliferating culture. However, significant amounts of integrated ($4.2 \times 10^5 \pm 5.4 \times 10^4$ copies per culture) and 2LTR ($1.5 \times 10^5 \pm 1.5 \times 10^3$ copies per culture) form DNA were found in the arrested culture (Fig. 1B). Similar results were also obtained in APH-treated 293T cells (data not shown). These data correspond well with the previously reported findings of the high susceptibility of APH-treated cells to HIV-1 [3,22]. Importantly, the ratios of integrated form and 2LTR form to full-length/1LTR form were similar in the proliferating (integrated; 0.108 ± 0.024, 2LTR; 0.022 ± 0.002, full-length/1LTR; 1.0) and the arrested cultures (integrated; 0.09 ± 0.011, 2LTR; 0.031 ± 0.001, full-length/1LTR; 1.0), respectively, strongly suggesting that HIV-1 cDNA efficiently traverse NPC, depending on the active nuclear import machinery in not only non-dividing cells but also proliferating cells.

3.2. Inhibition of HIV-1 cDNA import with a Nup98-specific inhibitor

Next, to examine the specificity of our real-time PCR assay and the associated molecules in nuclear entry of HIV-1 cDNA, we prepared HIV reverse transcription-inhibited (AZT-treated), transcription-blocked (ActD-treated), or CRM1-dependent nuclear export-inhibited (LMB-treated) 293T cell cultures. As expected, AZT significantly inhibited the appearance of all forms of DNA (Fig. 2A a–c). Although dose-dependent inhibition of integration was found in ActD- or LMB-treated cultures, significant accumulation of the 2LTR form was also found (Fig. 2A f and i), suggesting that newly synthesized proteins as well as CRM1-dependent exported proteins may be required for the efficient integration but not nuclear entry of HIV-1 cDNA. To examine whether specific Nups are required for HIV infection, we used VSV M protein, a specific inhibitor protein against Nup98. It has been shown that Nup98 is involved in the nuclear import of some proteins as well as the export of RNA, and its function is specifically impaired in the presence of VSV M protein [20]. The VSV M binds a region within residues 66–515 of Nup98 that encompasses most of the FG repeats, the hRAE1/Gle2 binding site or GLEBS-like motif [23], and most of the predicted glycosylation sites of the Nups. Through these sites, Nup98 was able to interact with three

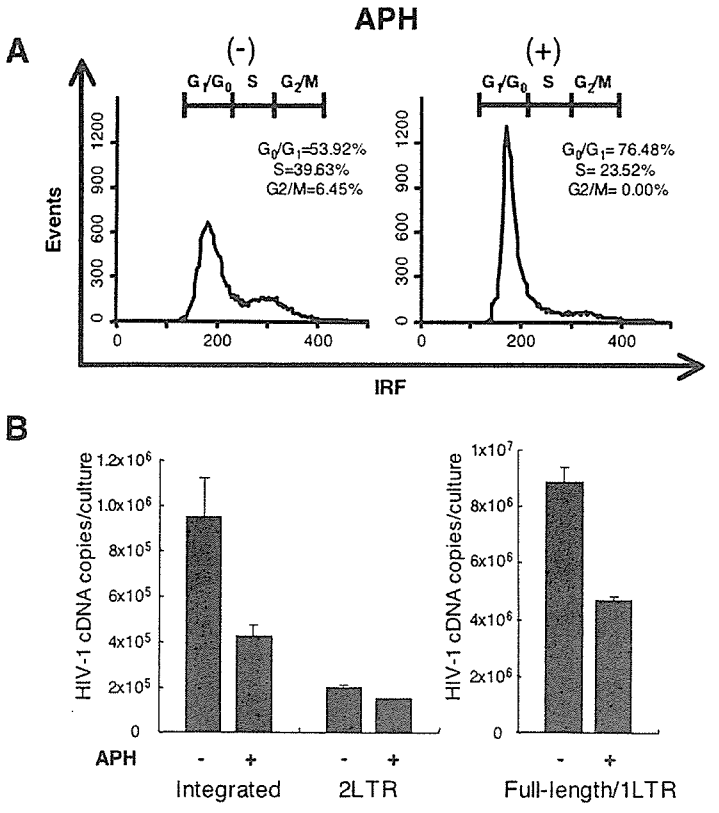

Fig. 1. Efficient nuclear entry of HIV-1 cDNA in arrested cells. (A) Cell-cycle analysis of APH-treated and -untreated cells. MT-2 cells were incubated for 24 h without (–) or with (+) APH, and then analyzed for DNA content by flow cytometry of proridium iodide-stained nuclei. Representative flow cytometry data from one of three independent experiments is shown. (B) Quantification of HIV-1 cDNA after HIV-1 vector infection in APH-treated and -untreated cells. Number of viral DNA copies per culture (baseline cell number is 2×10^5 cells) is indicated. APH-treated or -untreated MT-2 cells were infected with HIV-1 vector, and cultured without (–) or with (+) APH for another 24 h, respectively. Then, DNA was extracted and subjected to PCR assay. Results are mean ± S.D. of three independent experiments.

putative Nup98 partners: RAE1 [23], CRM1 [24], and TAP [25]. VSV M-mediated inhibition was not observed in a site-directed mutant (residue 52–54), termed VSV M(D) [20]. We used the VSV M as a specific inhibitor of the Nup98 function. An obvious impairment of integrated and 2LTR but not full-length DNA was found in only the wild-type but not the mutant VSV M(D)-transfected culture (Fig. 2B). This impairment was restored with ectopic overexpression of Nup98 (pcDNup98) (Fig. 2B, lane 5). Western blotting indicated that the overexpressed Nup98 was co-precipitated with VSV M but not VSV M(D) protein (Fig. 2C), suggesting that the overexpressed Nup98 absorbed VSV M protein, and the Nup98 function was recovered. Thus, Nup98 may have a role in nuclear import of HIV cDNA.

3.3. Depletion of Nup98 by siRNA

Next, to examine directly the involvement of Nup98 in HIV-1 cDNA nuclear import, Nup98 was depleted by the siRNA technique. After transfection with Nup98-specific siRNA-expressing plasmid, mRNA expression of Nup98 as well as Nup96, generated from the same precursor transcripts of Nup98 [26], but not other Nups such as p62, Nup107, Nup153, and Nup214, were specifically inhibited (Fig. 3A). It was also confirmed that the level of ectopic Nup98 protein expression was inhibited with the siRNA-expressing plasmid as it was lower than that in its endogenous expression (Fig. 3B). Immunofluorescence analysis using an anti-Nup98 antibody also confirmed the significant inhibition of Nup98 expression on nuclear membrane in the Nup98 siRNA-targeted HeLa cells using a siRNA-expressing lentivirus vector (Fig. 3C, upper panel). We further examined the distribution of NPC components using mAb414, an antibody known to interact with many FG-containing Nups, mainly p62 and to a less degree, Nup153, Nup214, and Nup358 but not Nup98. The Nup98 siRNA-transduced cells exhibited weak mAb414-labeling intensity at the nuclear rim and shift of labeling to the cytoplasm, probably cytoplasmic annulate lamellae (Fig. 3C, lower panel). However, the total amount of p62 (main component of NPC) was similar in both Nup98-siRNA-targeted or control cultures (Fig. 3D). A previous study using Nup98 knockout mice indicated that Nup98 is essential for rapid cell proliferation but dispensable for basal cell growth and some specific destruction of NPC component [27]. The Nup98-knockout cell was reported to have a thin nuclear envelope as well as many cytoplasmic annulate lamellae. Our Nup98-siRNA-targeted cells had similar structures. It was also reported that the mutant pores of the knockout cells were clearly impaired in in vitro transport